protein at normal and elevated temperature. *J. Mol. Graph. Model.* 20: 145–154.

Glockshuber, R., S. Homemann, R. Riek, G. Wider, M. Billeter, and K. Wuthrich. 1997. Three-dimensional NMR structure of a self-folding domain of the prion protein PrP(121–231). *Trends Biochem. Sci.* 22: 241–242.

Gsponer, J., P. Ferrara, and A. Caflisch. 2001. Flexibility of the murine prion protein and its Asp178Asn mutant investigated by molecular dynamics simulations. *J. Mol. Graph. Model.* 20:169–182.

Guilbert, C., F. Ricard, and J. C. Smith. 2000. Dynamic simulation of the mouse prion protein. *Biopolymers.* 54:406–415.

Hansson, T., C. Oostenbrink, and W. F. van Gunsteren. 2002. Molecular dynamics simulations. *Curr. Opin. Struct. Biol.* 12:190–196.

Herrmann, L. M., and B. Caughey. 1998. The importance of the disulfide bond in prion protein conversion. *Neuroreport.* 9:2457–2461.

Higo, J., N. Ito, M. Kuroda, S. Ono, N. Nakajima, and H. Nakamura. 2001. Energy landscape of a peptide consisting of alpha-helix, 3(10)-helix, beta-turn, beta-hairpin and other disordered conformations. *Protein Sci.* 10:1160–1171.

Hori, A., H. Tezuka, Y. Ishikawa, N. Soda, H. Konaka, and M. Maeda. 1996. Implementation of gang-scheduling on workstation cluster. *In* IPPS'96 Workshop on Job Scheduling Strategies for Parallel Processing, Vol. 1162 of Lecture Notes Computer Science. D. G. Feitelson and L. Rudolph, editors. Springer-Verlag. 76–83.

Homemann, S., and R. Glockshuber. 1998. A scrapie-like unfolding intermediate of the prion protein domain PrP(121–231) induced by acidic pH. *Proc. Natl. Acad. Sci. USA.* 95:6010–6014.

Jorgensen, W., J. Chandreskhar, J. Madura, R. Imprey, and M. Klein. 1983. Comparison of simple potential functions for simulating water. *J. Chem. Phys.* 79:926–935.

Kabsch, W., and C. Sander. 1983. Dictionary of protein secondary structure: pattern recognition of hydrogen-bonded and geometrical features. *Biopolymers.* 22:2577–2637.

Kaneko, K., L. Zulianello, M. Scott, C. M. Cooper, A. C. Wallace, T. L. James, F. E. Cohen, and S. B. Prusiner. 1997. Evidence for protein X binding to a discontinuous epitope on the cellular prion protein during scrapie prion propagation. *Proc. Natl. Acad. Sci. USA.* 94:10069–10074.

Knaus, K. J., M. Morillas, W. Swietnicki, M. Malone, W. K. Surewicz, and V. C. Yee. 2001. Crystal structure of the human prion protein reveals a mechanism for oligomerization. *Nat. Struct. Biol.* 8:770–774.

Kocisko, D. A., S. A. Priola, G. J. Raymond, B. Chesebro, P. T. Lansbury, Jr., and B. Caughey. 1995. Species specificity in the cell-free conversion of prion protein to protease-resistant forms: a model for the scrapie species barrier. *Proc. Natl. Acad. Sci. USA.* 92:3923–3927.

Kollman, P. A., R. Dixon, W. Cornell, T. Fox, C. Chipot, and A. Pohorille. 1997. The development/application of a 'minimalist' organic/biochemical molecular mechanic force field using a combination of ab initio calculations and experimental data. *In* Computer Simulation of Biomolecular Systems, Vol. 3. A. Wilkinson, P. Weiner, and W. F. van Gunsteren, editors. Elsevier. 83–96.

Koradi, R., M. Billeter, and K. Wüthrich. 1996. MOLMOL: a program for display and analysis of macromolecular structures. *J. Mol. Graph.* 14: 51–55.

Korth, C., B. Stierli, P. Streit, M. Moser, O. Schaller, R. Fischer, W. Schulz-Schaeffer, H. Kretzschmar, A. Raeber, U. Braun, F. Ehrensperger, S. Homemann, R. Glockshuber, R. Riek, M. Billeter, K. Wuthrich, and B. Oesch. 1997. Prion (PrPSc)-specific epitope defined by a monoclonal antibody. *Nature.* 390:74–77.

Lansbury, P. T., Jr., and B. Caughey. 1995. The chemistry of scrapie infection: implications of the 'ice 9' metaphor. *Chem. Biol.* 2:1–5.

Lopez, G. F., R. Zahn, R. Riek, and K. Wuthrich. 2000. NMR structure of the bovine prion protein. *Proc. Natl. Acad. Sci. USA.* 97:8334–8339.

Maiti, N. R., and W. K. Surewicz. 2001. The role of disulfide bridge in the folding and stability of the recombinant human prion protein. *J. Biol. Chem.* 276:2427–2431.

Meyer, R. K., A. Lustig, B. Oesch, R. Fatzer, A. Zurbriggen, and M. Vandevelde. 2000. A monomer-dimer equilibrium of a cellular prion protein (PrPC) not observed with recombinant PrP. *J. Biol. Chem.* 275:38081–38087.

Monod, J., J. Wyman, and J.-P. Changeux. 1965. On the nature of allosteric transitions: a plausible model. *J. Mol. Biol.* 12:88–118.

Muramoto, T., M. Scott, F. E. Cohen, and S. B. Prusiner. 1996. Recombinant scrapie-like prion protein of 106 amino acids is soluble. *Proc. Natl. Acad. Sci. USA.* 93:15457–15462.

Okimoto, N., K. Yamanaka, A. Suenaga, M. Hata, and T. Hoshino. 2002. Computational studies on prion proteins: effect of $Ala^{117} \rightarrow Val$ mutation. *Biophys. J.* 82:2746–2757.

Pan, K. M., M. Baldwin, J. Nguyen, M. Gasset, A. Serban, D. Groth, I. Mehlehorn, Z. Huang, R. J. Fletterick, F. E. Cohen, and S. B. Prusiner. 1993. Conversion of alpha-helices into beta-sheets features in the formation of the scrapie prion proteins. *Proc. Natl. Acad. Sci. USA.* 90:10962–10966.

Parchment, O., and J. Essex. 2000. Molecular dynamics of mouse and Syrian hamster PrP: implications for activity. *Proteins* 38:327–340.

Peretz, D., R. A. Williamson, Y. Matsunaga, H. Serban, C. Pinilla, R. B. Bastidas, R. Rozenshteyn, T. L. James, R. A. Houghten, F. E. Cohen, S. B. Prusiner, and D. R. Burton. 1997. A conformational transition at the N terminus of the prion protein features in formation of the scrapie isoform. *J. Mol. Biol.* 273:614–622.

Prusiner, S. B. 1982. Novel proteinaceous infectious particles cause scrapie. *Science.* 216:136–144.

Prusiner, S. B. 1991. Molecular biology of prion diseases. *Science* 252:1515–1522.

Prusiner, S. B. 1996. Molecular biology and pathogenesis of prion diseases. *Trends Biochem. Sci.* 21:482–487.

Riek, R., S. Homemann, G. Wider, M. Billeter, R. Glockshuber, and K. Wuthrich. 1996. NMR structure of the mouse prion protein domain PrP(121–321). *Nature.* 382:180–182.

Riek, R., G. Wider, M. Billeter, S. Homemann, R. Glockshuber, and K. Wuthrich. 1998. Prion protein NMR structure and familial human spongiform encephalopathies. *Proc. Natl. Acad. Sci. USA.* 95:11667–11672.

Riley, M. L., C. Leucht, S. Gauczynski, C. Hundt, M. Brecelj, G. Dodson, and S. Weiss. 2002. High-level expression and characterization of a glycosylated covalently linked dimer of the prion protein. *Protein Eng.* 15:529–536.

Ryckaert, J. P., G. Ciccotti, and H. J. C. Berendsen. 1977. Numerical integration of the Cartesian equations of motion of a system with constraints: molecular dynamics of *n*-alkanes. *J. Comput. Phys.* 23:327–341.

Safar, J., P. P. Roller, D. C. Gajdusek, and C. J. Gibbs. 1993. Thermal stability and conformational transitions of scrapie amyloid (prion) protein correlate with infectivity. *Protein Sci.* 2:2206–2216.

Swietnicki, W., R. Petersen, P. Gambetti, and W. K. Surewicz. 1997. pH-dependent stability and conformation of the recombinant human prion protein PrP(90–231). *J. Biol. Chem.* 272:27517–27520.

Telling, G. C., M. Scott, J. Mastrianni, R. Gabizon, M. Torchia, F. E. Cohen, S. J. DeArmond, N. Stahl, and S. B. Prusiner. 1995. Prion propagation in mice expressing human and chimeric PrP transgenes implicates the interaction of cellular PrP with another protein. *Cell.* 83: 79–99.

Tompa, P., G. E. Tusnady, P. Friedrich, and I. Simon. 2002. The role of dimerization in prion replication. *Biophys. J.* 82:1711–1718.

Viles, J. H., D. Donne, G. Kroon, S. B. Prusiner, F. E. Cohen, H. J. Dyson, and P. E. Wright. 2001. Local structural plasticity of the prion protein. Analysis of NMR relaxation dynamics. *Biochemistry.* 40:2743–2753.

Welker, E., L. D. Raymond, H. A. Scheraga, and B. Caughey. 2002. Intramolecular versus intermolecular disulfide bonds in prion proteins. *J. Biol. Chem.* 277:33477–33481.

Welker, E., W. J. Wedemeyer, and H. A. Scheraga. 2001. A role for intermolecular disulfide bonds in prion diseases? *Proc. Natl. Acad. Sci. USA* 98:4334–4336.

Westbrook, J., Z. Feng, S. Jain, T. N. Bhat, N. Thanki, V. Ravichandran, G. L. Gilliland, W. Bluhm, H. Weissig, D. S. Greer, P. E. Bourne, and H. M. Berman. 2002. The Protein Data Bank: unifying the archive. *Nucleic Acids Res.* 30:245–248.

Wong, N. K. C., D. V. Renouf, S. Lehmann, and E. F. Hounsell. 2000. Glycosylation of prions and its effect on protein conformation relevant to amino acid mutations. *J. Mol. Graph. Model.* 18:126–134.

Zahn, R., A. Liu, T. Luhrs, R. Riek, C. von Schroetter, F. L. Garcia, M. Billeter, L. Calzolai, G. Wider, and K. Wuthrich. 2000. NMR solution structure of the human prion protein. *Proc. Natl. Acad. Sci. USA.* 97: 145–150.

Zhang, H., J. Stockel, I. Mehlhorn, D. Groth, M. A. Baldwin, S. B. Prusiner, T. L. James, and F. E. Cohen. 1997. Physical studies of conformational plasticity in a recombinant prion protein. *Biochemistry.* 36: 3543–3553.

Zuegg, J., and J. E. Greedy. 1999. Molecular dynamics simulations of human prion protein: importance of correct treatment of electrostatic interactions. *Biochemistry.* 38:13862–13876.

ACADEMIC PRESS

Available online at www.sciencedirect.com

SCIENCE DIRECT®

Biochemical and Biophysical Research Communications 305 (2003) 1034–1039

BBRC

www.elsevier.com/locate/ybbrc

Stimulation of cellular prion protein expression by TSH in human thyrocytes☆

Kazuko Yamazaki,[a] Emiko Yamada,[a] Yoshio Kanaji,[a] Tetsuo Yanagisawa,[b] Yoshiyuki Kato,[b] Kanji Sato,[b,*] Kazue Takano,[b] Yuji Sakasegawa,[c,d] and Kiyotoshi Kaneko[c,d]

[a] *Thyroid Disease Institute, Kanaji Hospital, Kita-ku, Tokyo 114-0015, Japan*

[b] *Department of Medicine, Institute of Clinical Endocrinology, Tokyo Women's Medical University, Kawada-cho 8-1, Shinjuku-ku, Tokyo 162-8666, Japan*

[c] *Department of Cortical Function Disorders, National Institute of Neuroscience, National Center of Neurology and Psychiatry, Kodaira, Tokyo 187-8502, Japan*

[d] *Core Research for Evaluational Science and Technology (CREST), Japan Science and Technology Corporation, Kawaguchi, Saitama 332-0012, Japan*

Received 29 March 2003

Abstract

The cellular isoform of prion protein (PrP^C) is a cell-surface glycosyl-phosphatidylinositol-anchored protein which is ubiquitously expressed on the cell membrane. It may function as a cell receptor or as a cell adhesion molecule. Thyroid follicles, obtained from patients with Graves' disease at thyroidectomy, were cultured in F-12/RPMI-1640 medium supplemented with 0.5% fetal bovine serum and bovine thyroid stimulating hormone (bTSH). Northern blot analyses revealed that bTSH increased the steady-state expression levels of PrP mRNA in a time- and dose-dependent manner. This increase was reproduced by dibutyryl-cAMP and 12-decanoylphorbol-13-acetate. The mRNA expression was greater in thyroid follicles in suspension culture than in thyrocytes cultured in a monolayer. These findings suggest that TSH stimulates PrP mRNA expression in thyrocytes through the protein kinase A and C pathways. The greater mRNA expression in thyroid follicles than in monolayer cells suggests that PrP^C may be involved in structure formation or maintenance of thyroid follicles.

Keywords: Prion protein; Thyroid; TSH; cDNA microarray

Prion protein (PrP) exists in two isoforms: a cellular isoform (PrP^C) rich in α-helices and a disease isoform (PrP^{Sc}) rich in β-sheet structures [1,2]. It is well established that a post-translationally modified isoform of PrP^C (PrP^{Sc}) is involved in the pathogenesis of Creutzfeldt–Jakob disease in humans, bovine spongiform encephalopathy in cattle, scrapie in sheep, and all other known transmissible spongiform encephalopathies [1,2].

In all natural and experimental prion diseases, PrP^{Sc} accumulates in the central nervous system, resulting in neurological dysfunction. PrP^C is present in all vertebrates so far examined, is widely expressed during embryogenesis, and has been strongly conserved throughout evolution [3]. Since PrP^C is a glycosyl-phosphatidylinositol-anchored cell surface protein, its physiological role could be related to ligand uptake, cell adhesion, and recognition of cell signaling [1,2]. These possibilities have been extensively studied, but the normal function of this housekeeping gene is still poorly understood.

PrP^C is expressed predominantly in the brain, but also in a wide variety of peripheral tissues and cells, including lung, skeletal muscle, heart, uterus, thymus,

☆ *Abbreviations:* PrP^C, cellular form of prion protein; PrP^{Sc}, infectious 'scrapie' form of prion protein; bTSH, bovine thyroid stimulating hormone; dbcAMP, dibutyryl-cAMP; TPA, 12-decanoyl-phorbol-13-acetate.

* Corresponding author. Fax: +81-3-3354-3706.
E-mail address: satokan@attglobal.net (K. Sato).

0006-291X/03/$ - see front matter © 2003 Elsevier Science (USA). All rights reserved.
doi:10.1016/S0006-291X(03)00801-5

tongue, skin, gastrointestinal tract, pancreas, eye, sperm, circulating mononuclear cells, and macrophages at a relatively low level [4–9]. However, PrP^C metabolism in these non-neuronal tissues, especially in endocrine tissues, remains entirely unknown.

By using a cDNA microarray which can analyze 2400 genes in a single run, we demonstrated that thyroid stimulating hormone (TSH) upregulated more than 200 genes in cultured human thyroid follicles [10]. Among them, we have found that PrP mRNA was strongly expressed even at a basal level and its expression level was increased 3-fold by TSH stimulation (unpublished observation). Therefore, we used Northern and Western blot analyses to examine the regulatory mechanism of PrP^C expression in cultured human thyroid follicles derived from patients with Graves' disease.

Materials and methods

After informed consent had been obtained, thyroid glands were obtained from Graves' patients scheduled for subtotal thyroidectomy. Human neuroblastoma cells (NB9 and NB69) [11] and leukemia cells (K562) were supplied by RIKEN Cell Bank (Tsukuba Science City, Japan). These cells were used as positive (NB9 and NB69) and negative (K562) controls [12,13]. Mouse neuroblastoma cells (N2a) were also used as a positive control [14]. Dibutyryl cAMP (dbcAMP) and 12-decanoylphorbol-13-acetate (TPA) were purchased from Sigma–Aldrich (Tokyo, Japan).

Suspension and monolayer culture of human thyroid follicles. Thyroid follicles were prepared by digestion with collagenase and dispase as described previously [15–18]. In brief, thyroid tissue (15–30 g) obtained as above was minced into small pieces with scissors. The prepared tissue was then digested with 0.3 mg/mL collagenase (type 4; Sigma Chemical, Tokyo, Japan) and 5 mg/mL dispase (Godo Shusei, Tokyo, Japan) in Hanks' balanced salt solution at 32 °C for 30 min. The digested material was filtered through a nylon mesh (80 mesh) and any undigested tissue fragments were processed a second time. The resulting filtrate, containing separated thyroid follicles, was centrifuged at 800 rpm for 1 min and then the pellet was washed three times with basal medium (F-12/RPMI-1640, 1:1) supplemented with 0.5% fetal bovine serum and NaI (10^{-8} M) until it became white. By this mild centrifugation procedure, thyroid follicles were separated from erythrocytes and mononuclear cells, although a few immunocompetent cells in the thyroid follicles could not be removed [18]. Then thyroid follicles suspended in 15 mL of basal medium (about 1000–2000 follicles/mL) were added to 10-cm dishes, the bottom of which had been coated with agarose. After 2–3 days of preculture, the medium was changed and the thyroid follicles were cultured with or without bovine thyroid stimulating hormone (bTSH) (100 μU/mL) for 2 additional days. In other experiments, thyroid follicles were precultured in basal medium for 2–3 days and in fresh basal medium for an additional 24 h, and then cultured in fresh basal medium containing 100 μU/mL bTSH. On the following day, NaI solution (10^{-3} M) was added to a final concentration of 10^{-5} M. To the control culture, only distilled water (150 μL) was added. After the culture medium had been gently mixed, the thyroid follicles were cultured for an additional 24 h in the presence of bTSH (100 μU/mL). At this high NaI concentration, T3 synthesis and release were suppressed almost completely by Wolff–Chaikoff effects, as reported previously [18]. In a few experiments, thyroid follicles were cultured in uncoated culture dishes so that they adhered to and grew on the bottom of the dishes, forming a cell monolayer after a few days. Human neuroblastoma cells (NB9 and NB69), human leukemia cells (K562), and mouse neuroblastoma cells (N2a) were cultured on non-coated 10-cm plates to near confluency.

cDNA microarray analysis. Total RNA was converted to cDNA using a Human cDNA System I Direct Kit (NEN Life Science Products, Boston, MA) as described previously [10]. cDNA obtained from thyroid follicles cultured in the control and treated media was labeled with Cy5 (red) and Cy3 (green), respectively, and expression levels of 2400 genes were analyzed using a cDNA microarray (Micromax human cDNA microarray system, NEN Life Science Products). Laser detection of the Cy3 and Cy5 signals on the microarray was performed with a non-confocal laser reader (Gene PX 4000A; Axon Instruments, Union, CA). Fluorescence signal intensities and the Cy3/Cy5 ratios for each of the 2400 cDNAs were analyzed by the Gene PixPro 30 software package (Axon Instruments).

Northern blot hybridization. Total RNA (10 μg) was size-fractionated in 1% agarose gels containing 3.3% formaldehyde and transferred to nylon membranes (Nytran; Schleicher and Schull, Dassel, Germany). A probe molecule covering 100–669 nucleotides of the PrP open reading frame was synthesized by polymerase chain reaction from pBS-huPrP. The PrP open reading frame was amplified from a human genomic library (Takara Bio, Otsu, Shiga, Japan), cloned into pBluescriptII SK+ (Stratagene, La Jolla, CA), and labeled with ^{32}P using Takara Random Primer DNA Labeling Kit ver. 2.0 (Takara Biochemicals, Tokyo, Japan). Northern blot hybridization was performed under high-stringency conditions as described previously [16].

Western blotting. Cells were lysed in a buffer containing 1% Nonidet P-40 and 1% SDS buffer. SDS–PAGE and Western transfer to nitrocellulose membranes were performed under standard conditions. Membranes were reacted with anti-PrP monoclonal antibodies (6H4; Prionics AG, Zürich, Switzerland) and then horseradish peroxidase-labeled sheep anti-mouse IgG (Amersham Biosciences, Little Chalfont, Buckinghamshire, UK). The antibody recognized human and murine PrP^C equipotently. The immunodecorated bands were visualized in an ECL Plus Detection System (Amersham Biosciences) and analyzed by Fluor-S MAX MultiImager (Bio-Rad Laboratories, Nercules, CA).

Results

cDNA microarray analysis

As we reported previously [10], cDNA microarray analysis revealed that a number of genes (>200) were upregulated by TSH. Representative genes were ATP synthase α-subunit, cytochrome *c* oxidase subunit, and PrP. The expression level of PrP was increased 3-fold when human thyroid follicles were cultured with 100 μU/mL bTSH for 2 days (Fig. 1A).

PrP mRNA expression by bTSH in human thyroid follicles

Consistent with the data obtained from cDNA microarray analysis, Northern blot hybridization revealed that human thyroid follicles constitutively expressed PrP mRNA (2.7 kb), and that its steady-state expression levels were increased nearly 3-fold by TSH (Fig. 1B, left panel). Western blot hybridization also confirmed that TSH increased PrP^C protein to the same extent (Fig. 1B, right panel).

Although K562 cells are reported to produce little PrP^C [13], our Northern blot hybridization revealed a

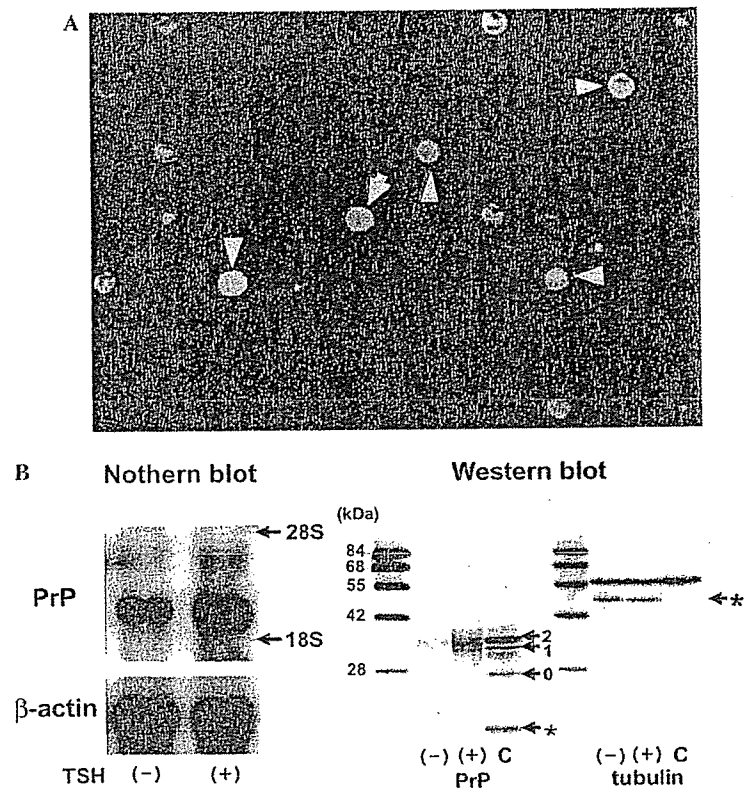

Fig. 1. PrP mRNA and protein expression in human thyroid follicles by TSH. (A) Human thyroid follicles were suspension-cultured in the presence or absence of 100 μU/mL bTSH for 2 days. Total RNA from these cells was prepared and used for cDNA microarray analysis. The genes upregulated by TSH displayed green fluorescence such as prion (arrow), ATP synthase α subunit (upward arrowhead), and cytochrome *c* oxidase (leftward arrowhead), whereas those suppressed by TSH displayed red fluorescence (not shown in this panel). Those not modulated by TSH displayed yellow fluorescence such as ribosomal protein L32 (downward arrowhead) and L29 (rightward arrowhead). (B) Total RNA in (A) was also analyzed by Northern blot hybridization. A specific hybridization signal was detected at approximately 2.7 kb (left panel). Simultaneously, 20 μg of cell extracts from thyroid follicles with or without bTSH or mouse N2a neuroblastoma cells was analyzed by Western blotting using monoclonal antibodies against PrP (6H4) and tubulin (right panel). 0, 1, 2: non-, mono-, or di-glycosylated prion proteins; *: degradation products; and C: Mouse Na2 neuroblastoma cells.

faint band of PrP mRNA expression (Fig. 2A). The TSH-induced PrP mRNA expression levels in thyroid follicles were much greater than those in the human neuroblastoma cell line NB69 and K562 cells, and comparable to those of the human neuroblastoma cell line NB9 (Fig. 2A).

TSH increased the steady-state expression levels of PrP mRNA in a concentration-dependent manner: the minimum TSH concentration required to induce PrP mRNA expression was 10 μU/mL (Fig. 2B). bTSH increased PrP mRNA expression in a time-dependent manner: when thyroid follicles were cultured with 100 μU/mL bTSH for 1, 3, 6, 24, and 48 h, PrP mRNA expression levels increased 1.3-, 3.5-, 2.4-, 2.0-, and 2.4-fold, respectively (Fig. 2C).

A TSH-mediated increase in PrP mRNA expression was also reproduced by a protein kinase A effector, dbcAMP, which increased PrP mRNA expression at 1 mM (Fig. 2D, left panel). At this concentration, thyroid hormonogenesis was observed (data not shown). A protein kinase C effector, TPA, also increased the PrP expression levels in a concentration-dependent manner at 10^{-8}–10^{-6} M (Fig. 2D, right panel).

When thyroid follicles were cultured with various concentrations of iodide (10^{-8}–10^{-5} M), iodide did not modulate PrP mRNA expression levels, although thyroid hormonogenesis was almost completely suppressed at 10^{-5} M (data not shown).

In four experiments, TSH-induced expression levels of PrP mRNA in human thyroid follicles in suspension culture were compared with those in monolayer cells. The monolayer cells were formed during several days of culture from thyroid follicles on culture dishes which had not been coated with agarose. bTSH at 100 μU/mL increased the steady-state expression levels of PrP mRNA 2.5 ± 0.24-fold in thyroid follicles in suspension culture, but only 1.5 ± 0.4-fold in monolayer cells ($P < 0.05$) (Fig. 3).

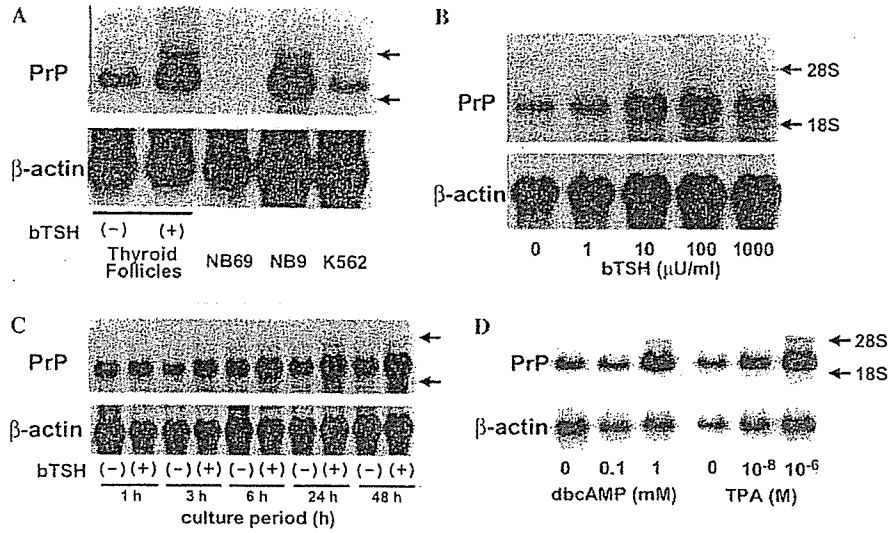

Fig. 2. Effect of dbcAMP and TPA on PrP mRNA in human thyroid follicles. (A) Thyroid follicles were suspension-cultured in the presence or absence of 100 μU/mL bTSH for 2 days. Human neuroblastoma cells (NB9 and NB69) and human leukemia cells (K562) were also cultured until they reached confluency. (B) Thyroid follicles were suspension-cultured at various concentrations (1–100 μU/mL) of bTSH for 2 days. (C) Thyroid follicles were suspension-cultured for 1, 3, 6, 24, or 48 h in the presence or absence of 100 μU/mL bTSH. Total RNA from these cells was analyzed by Northern blot hybridization. (D) Thyroid follicles were suspension-cultured in the presence of dbcAMP for 24 h or TPA for 3 h. Total RNA from these cultures was analyzed by Northern blot hybridization.

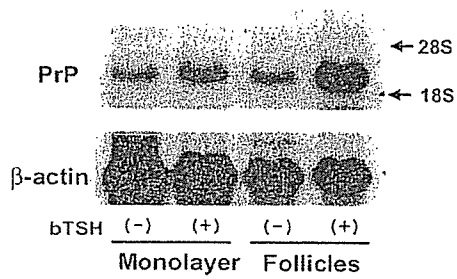

Fig. 3. Effect of bTSH on PrP mRNA expression in human thyrocytes in monolayer and follicles. Thyroid follicles were cultured in monolayer or in suspension in the presence or absence of bTSH (100 μU/mL) for 2 days. Total RNAs from these cells were analyzed by Northern blot hybridization.

Discussion

Sheep thyroid gland is considered a safe organ against bovine spongiform encephalopathy infection, but no data have been collected from human thyroid tissues so far. By using a cDNA microarray, Northern blot hybridization, and Western blot analysis, we have demonstrated that PrP^{C}, a precursor of PrP^{Sc}, is constitutively expressed in human thyroid follicles at levels comparable to those in a human neuroblastoma cell line. Furthermore, PrP mRNA expression is stimulated by TSH through the protein kinase A and C pathways. Among various endocrine tissues examined up to now, PrP^{C} expression has been described only in adrenal tissues [4,19], which are known to be infectious [19]. Although there is no firm evidence for the presence of PrP^{Sc} and its derivatives in human thyroid tissue, our data suggest a potential risk of human thyroid derivatives in prion infection.

Although the physiological function of PrP^{C} is not well elucidated, an increasing number of reports suggest that PrP mRNA expression levels are regulated by growth factors and differentiation-regulating factors. An in vivo study has revealed that nerve growth factor (NGF) increases PrP mRNA levels in developing hamster brain [20]. In SV40-transformed neuronal progenitor cells, differentiating agents such as dbcAMP and phorbol-12-myristate 13-acetate (PMA) increased PrP mRNA and protein expression before the cells developed into neuronal-like cells [21]. Furthermore, NGF and insulin induced cell differentiation and enhanced the expression of PrP mRNA [22]. GH and IGF-I also induced a dose-dependent increase of PrP mRNA in a rat pheochromocytoma cell line (PC-12) [23]. PrP mRNA is expressed in human keratinocytes and its expression levels are increased by TGF-β and interferon-γ [24]. Our results are consistent with those indicating that growth factors exert stimulatory effects on PrP mRNA production in neuronal cells. Since TSH signals are transferred through the protein kinase A and C pathways [25], it is reasonable that dbcAMP and TPA also increased the PrP mRNA expression levels in thyroid follicles.

PrP knock-out mice show no obvious developmental defects or behavioral abnormalities over nearly 2 years [1,2], suggesting that thyroid function in these mice is not dramatically altered. On the other hand, experiments with target-directed disruption of the PrP gene

have revealed that PrP^C might be involved in synaptic transmission in nerve cells [26] or in sleep regulation [27]. PrP^C is also expressed in lymphocytes, where it is involved in T cell activation [28]. PrP^C might protect human neurons against Bax-mediated apoptosis [29]. Despite intensive research, the function and metabolism of PrP^C in non-neuronal, non-lymphoid tissues, including endocrine tissues, are entirely unknown.

In most cells, PrP^C is localized on the cell surface as a glycosyl-phosphatidylinositol-anchored protein. The greater expression of PrP mRNA in thyroid follicles than in monolayer cells suggests that PrP^C may play important roles in cell to cell interaction, differentiation of cells, or maintenance of thyroid follicle architecture. Consistent with our observations, neuroblastoma cells overexpressing PrP (N2a), when cultured in suspension, are reported to adhere to each other and form aggregates [30]. This aggregation is reduced after phosphatidylinositol-specific phospholipase C mediated release of the protein and by pre-incubation of the cells with an antibody raised against PrP^C, suggesting that PrP functions as an intercellular adhesion molecule and a cell surface ligand or receptor [30].

In conclusion, we have demonstrated that PrP mRNA and PrP^C are expressed in human thyrocytes, and that TSH stimulates PrP mRNA expression in thyrocytes through the protein kinase A and C pathways. The greater mRNA expression in thyroid follicles than in monolayer cells suggests that PrP^C may be involved in structure formation or maintenance of thyroid follicles. Although any physiological functions of PrP in endocrine tissues remain unknown, our in vitro data suggest that TSH regulates PrP^C expression in thyrocytes, as NGF does in neuronal cells.

Acknowledgments

This work was supported by grants from the Ministry of Education, Culture, Sports, Science and Technology of Japan (15590985), the Ministry of Health, Labour and Welfare of Japan (14161301), and CREST (Core Research for Evolutional Science and Technology) of Japan Science and Technology Corporation (34100).

References

[1] S.B. Prusiner, Prions, Proc. Natl. Acad. Sci. USA 95 (1998) 13363–13383.
[2] S.B. Prusiner, P. Peters, K. Kaneko, A. Taraboulos, V.F.E. Lingappa, F.E. Cohen, S.J. DeArmond, Cell biology of prions, in: S.B. Prusiner (Ed.), Prion Biology and Diseases, Cold Spring Harbor Laboratory Press, Cold Spring Harbor, NY, 1999, pp. 349–391.
[3] H.M. Schazl, M. Da Costa, L. Taylor, F.E. Cohen, S.B. Prusiner, Prion protein gene variation among primates, J. Mol. Biol. 245 (1995) 362–374.
[4] J.G. Fournier, Nonneuronal cellular prion protein, Int. Rev. Cytol. 208 (2001) 121–160.
[5] P.E. Bendheim, H.R. Brown, R.D. Rudelli, L.J. Scala, N.L. Goller, G.Y. Wen, R.J. Kascsak, N.R. Cashman, D.C. Bolton, Nearly ubiquitous tissue distribution of the scrapie agent precursor protein, Neurology 42 (1992) 149–156.
[6] J.G. Fournier, F. Escaig-Haye, T. Billette de Villemeur, O. Robain, C.I. Lasmezas, J.P. Deslys, D. Dormont, P. Brown, Distribution and submicroscopic immunogold localization of cellular prion protein (PrPc) in extracerebral tissues, Cell Tissue Res. 292 (1998) 77–84.
[7] M. Horiuchi, N. Yamazaki, T. Ikeda, N. Ishiguro, M. Shinagawa, A cellular form of prion protein (PrPc) exists in many non-neuronal tissues in sheep, J. Gen. Virol. 76 (1995) 2583–2587.
[8] M. Moudjou, Y. Frobert, J. Grassi, C. La Bonnardiere, Cellular prion protein status in sheep: tissue-specific biochemical signatures, J. Gen. Virol. 82 (2001) 2017–2024.
[9] P.J. Bosque, C. Ryou, G. Telling, D. Peretz, G. Legname, S.J. DeArmond, S.B. Prusiner, Prions in skeletal muscle, Proc. Natl. Acad. Sci. USA 99 (2002) 3812–3817.
[10] K. Yamazaki, E. Yamada, Y. Kanaji, T. Yanagisawa, Y. Kato, K. Takano, T. Obara, K. Sato, Genes regulated by TSH and iodide in cultured human thyroid follicles: analysis by cDNA microarray, Thyroid 13 (2003) 149–158.
[11] F. Gilbert, M. Feder, G. Balaban, D. Brangman, D.K. Lurie, R. Podolsky, V. Rinaldt, N. Vinikoor, J. Weisband, Human neuroblastomas and abnormalities of chromosomes 1 and 17, Cancer Res. 44 (1984) 5444–5449.
[12] J. Satoh, K. Kurohara, M. Yukitake, Y. Kuroda, Constitutive and cytokine-inducible expression of prion protein gene in human neural cell lines, J. Neuropathol. Exp. Neurol. 57 (1998) 131–139.
[13] Y. Bounhar, Y. Zhang, C.G. Goodyer, A. LeBlanc, Prion protein protects human neurons against Bax-mediated apoptosis, J. Biol. Chem. 276 (2001) 39145–39149.
[14] H. Baybutt, J. Manson, Characterisation of two promoters for prion protein (PrP) gene expression in neuronal cells, Gene 184 (1997) 125–131.
[15] K. Sato, T. Satoh, K. Shizume, M. Ozawa, D.C. Han, H. Imamura, T. Tsushima, H. Demura, Y. Kanaji, Y. Ito, T. Obara, Y. Fujimoto, Y. Kanaji, Y. Ito, Inhibition of ^{125}I organification and thyroid hormone release by interleukin-1, tumor necrosis factor-α, interferon-γ in human thyrocytes in suspension culture, J. Clin. Endocrinol. Metab. 70 (1990) 1735–1743.
[16] K. Sato, K. Yamazaki, K. Shizume, Y. Kanaji, T. Obara, K. Ohsumi, S. Yamaguchi, M. Shibuya, Stimulation of thyroid stimulating hormone and Graves' immunoglobulin G of vascular endothelial growth factor mRNA expression in human thyroid follicles in vitro and flt mRNA expression in the rat thyroid in vivo, J. Clin. Invest. 96 (1995) 1295–1302.
[17] K. Yamazaki, E. Yamada, Y. Kanaji, K. Shizume, D. Wang, N. Maruo, T. Obara, K. Sato, Interleukin-6 (IL-6) inhibits thyroid function in the presence of soluble IL-6 receptor in cultured human thyroid follicles, Endocrinology 137 (1996) 4857–4863.
[18] K. Nakajima, K. Yamazaki, E. Yamada, Y. Kanaji, S. Kosaka, K. Sato, K. Takano, Amiodarone stimulates interleukin-6 production in cultured human thyrocytes, exerting cytotoxic effects on thyroid follicles in suspension culture, Thyroid 11 (2001) 101–109.
[19] The European Agency for the Evaluation of Medical Products, Note for guidance on minimizing the risk of transmissing animal spongioform encephalopathy agents via human and veterinary medical products, London, 31 May 2001, EMEA/410/01 rev.1.
[20] W.C. Mobley, R.L. Neve, S.B. Prusiner, M.P. McKinley, Nerve growth factor increases mRNA levels for the prion protein and the β-amyloid protein precursor in developing hamster brain, Proc. Natl. Acad. Sci. USA 85 (1988) 9811–9815.

[21] C. Kuwahara, A. Kubosaki, T. Nishimura, Y. Nasu, Y. Nakamura, K. Saeki, Y. Matsumoto, T. Onodera, Enhanced expression of cellular prion protein gene by insulin or nerve growth factor in immortalized mouse neuronal precursor cell lines, Biochem. Biophys. Res. Commun. 268 (2000) 763–766.
[22] C. Lasmezas, J.P. Deslys, D. Dormont, Recombinant human growth hormone and insulin-like growth factor I induce PrP gene expression in PC12 cells, Biochem. Biophys. Res. Commun. 196 (1993) 1163–1169.
[23] P. Castelnau, F. Lazarini, J.P. Deslys, D. Dormont, Prion protein gene expression in cultured astrocytes treated by recombinant growth hormone and insulin-like growth factor, Exp. Neurol. 130 (1994) 407–410.
[24] J. Pammer, W. Weninger, E. Tschachler, Human keratinocytes express cellular prion-related protein in vitro and during inflammatory skin diseases, Am. J. Pathol. 153 (1998) 1353–1358.
[25] J.E. Dumont, F. Lamy, P. Roger, C. Maenhaut, Physiological and pathological regulation of thyroid cell proliferation and differentiation by thyrotropin and other factors, Physiol. Rev. 72 (1992) 667–697.
[26] S.B. Colling, J. Collinge, J.G. Jefferys, Hippocampal slices from prion protein null mice: disrupted Ca^{++}-activated K^{+} currents, Neurosci. Lett. 209 (1996) 49–52.
[27] I. Tober, S.E. Gaus, T. Deboer, P. Achenman, M. Fischer, T. Tuelicke, M. Moser, B. Oesch, P.A. McBride, J.C. Manson, Altered circadian rhythmus and sleep in mice devoid of prion protein, Nature 380 (1996) 639–642.
[28] N.A. Mabott, K.L. Brown, J. Manson, M.E. Bruce, T lymphocyte activation and the cellular form of the prion protein, Immunology 92 (1997) 161–165.
[29] Y. Bounhar, Y. Zhang, C.G. Goodyer, A. LeBlanc, Prion protein protects human neurons against Bax-mediated apoptosis, J. Biol. Chem. 276 (2001) 39145–39149.
[30] A. Mange, O. Milhavet, D. Umlauf, D. Harris, S. Lehmann, PrP-dependent cell adhesion in N2a neuroblastoma cells, FEBS Lett. 514 (2002) 159–162.

ELSEVIER

Physiology & Behavior 78 (2003) 303–309

PHYSIOLOGY & BEHAVIOR

Stress-induced impairment of inhibitory avoidance learning in female neuromedin B receptor-deficient mice

Kazuyuki Yamada[a,b,*,1], Yuko Santo-Yamada[a,c,1], Keiji Wada[a]

[a]*Department of Degenerative Neurological Diseases, National Institute of Neuroscience, National Center of Neurology and Psychiatry, 4-1-1 Ogawahigashi, Kodaira, Tokyo 187-8502, Japan*

[b]*Advanced Technology Development Center, Brain Science Institute, RIKEN, 2-1 Hirosawa, Wako, Saitama 351-0198, Japan*

[c]*Department of Mental Retardation and Birth Defect Research, National Institute of Neuroscience, National Center of Neurology and Psychiatry, 4-1-1 Ogawahigashi, Kodaira, Tokyo 187-8502, Japan*

Received 5 August 2002; received in revised form 15 October 2002; accepted 14 November 2002

Abstract

Neuromedin B (NMB) is a mammalian bombesin (BN)-like peptide that exerts its function via the neuromedin B receptor (NMB-R). The NMB/NMB-R system is involved in stress response, and therefore we examined behavioral properties in female mice lacking NMB-R using a restraint-induced stress paradigm. Thirty minutes of restraint in a wire mesh cage constituted a sufficient stress stimulus for mice as evidenced by elevated blood glucose concentrations in stressed wild-type and NMB-R-deficient mice. Using a one-trial passive avoidance test, stressed NMB-R-deficient mice exhibited a marked reduction in memory performance. NMB-R-deficient mice exhibited elevated spontaneous activity in a novel environment compared to non-stressed mutant mice after 30-min stress, and a similar difference was also observed between stressed/non-stressed wild-type mice. An elevated plus maze test showed that the stress stimulus had no effect on anxiety in either wild-type or NMB-R-deficient mice. Furthermore, pain response of wild-type and NMB-R-deficient mice induced by electric foot shock was not affected under either stressed or non-stressed conditions. These results indicate that impaired memory performance in stressed NMB-R-deficient mice is not a consequence of changes in spontaneous activity, anxiety, or pain response, and suggest that the NMB/NMB-R pathway may play a role in regulating the stress response via the neural system that controls learning and memory.

Keywords: Neuromedin B (NMB); Neuromedin B receptor (NMB-R); Restraint-induced stress; One-trial passive avoidance learning; Spontaneous activity; Blood glucose concentration; Elevated plus maze test; Pain response; Knockout mice

1. Introduction

Neuromedin B (NMB) is a bombesin (BN)-like peptide originally purified from porcine spinal cord [13]. NMB exerts its effects by binding the NMB receptor (NMB-R), a G-protein coupled receptor [19]. NMB affects various aspects of physiology and behavior, including thermoregulation [6], spontaneous activity [5], and feeding (for reviews see Refs. [12,22,24]). Mice lacking the NMB-R gene were generated [14] to facilitate studies of the involvement of the NMB/NMB-R system in behavior, and we recently reported that NMB-R-deficient mice exhibit altered anxiety-related behavior (risk assessment behavior in the light–dark box test and the elevated plus maze test) [23] as well as decreased defensive behavior (marble burying) [25]. One aspect of neuronal function involved in the behavioral changes in these mutant mice is abnormal 5-HT function [25]. It is widely known that dysfunction in the 5-HT system leads to behavioral abnormalities such as enhancement of both fear [4] and aggression [16]. Additionally, the 5-HT system plays a role in regulating stress response in animals [9]. Recently, several studies reported that BN-like peptides, including NMB, are involved in regulating stress response [8,10]. Furthermore, recent studies suggest that post-stress endocrine response (elevated plasma corticosterone concentration) is altered in male NMB-R-deficient mice [27] and stress-induced impairment of maternal behavior in female NMB-R-deficient mice [26]. Previous reports from our

* Corresponding author. Advanced Technology Development Center, Brain Science Institute, RIKEN, 2-1 Hirosawa, Wako, Saitama 351-0198, Japan. Tel.: +81-48-467-7659; fax: +81-48-467-6287.

E-mail address: kaz-yamada@brain.riken.go.jp (K. Yamada).

[1] These two authors equally contributed to this work.

0031-9384/02/$ – see front matter © 2002 Elsevier Science Inc. All rights reserved.
PII:S0031-9384(02)00979-4

laboratory as well as others prompted us to hypothesize that stress stimuli would uncover other behavioral alterations in this mutant mouse. Therefore, using female NMB-R-deficient mice, we conducted a series of experiments to examine the role of the NMB/NMB-R system in the regulation of the stress response, focusing particularly on the behavioral aspects of stress.

2. Materials and methods

2.1. Animals

Eighty-eight female NMB-R-deficient mice and 85 wild-type littermates were used as subjects (12–14 weeks of age, with mean body weights of 21.3±0.20 g for NMB-R-deficient and 21.8±0.16 g for wild-type mice). The NMB-R gene is autosomal. Female NMB-R-deficient mice and wild-type littermates were produced in our laboratory by mating NMB-R heterozygous males with NMB-R heterozygous females (F14: back crossed to C57BL/6J 14 times). Groups and sample sizes of mice as well as stress treatments are summarized in Table 1. Animal housing and all experiments were conducted in a temperature- and humidity-controlled room (23±2 °C, 60±5%). The light–dark cycle was 12 h:12 h (lights on at 0800 h). Mice were housed individually in ordinary plastic caging [JCL, CL-0103-1pc, 190 × ~260 × ~125 (h) mm] with wood shavings for at least 2 weeks prior to experimentation. Ordinary laboratory chow (JCL, CE-2, 342.2 kcal/100 g) and water were freely available to mice except during test situations. All behavioral experiments were performed between 1300 and 1700 h during the light cycle.

All animal experiments were performed in strict accordance with the guidelines of the National Institute of Neuroscience, National Center of Neurology and Psychiatry (Japan) and were approved by the Animal Investigation Committee of the Institute.

2.2. Experimental procedure

2.2.1. Administration of restraint stress

Mice assigned to stressed groups were restrained in a wire mesh cage (Natsume, Japan) for 30 min immediately prior to experimentation. The restraint was such that the mice could move slightly (to turn in the direction of their body only). On the other hand, mice assigned to non-stressed groups were simply handled, after which they were returned to their home cage for 30 min.

2.2.2. Blood glucose measurement

Blood was obtained by venesection at the tail tip using a fine glass blood collection tube coated with heparin (Terumo, Japan, VC-H075H). The tail veins were gently restricted using an apparatus for intravenous injection made of rubber, and about 50–70 μl of blood was collected within 15–30 s after restriction. The blood was immediately placed into an i-STAT cartridge (EC6+; i-STAT, USA) and the glucose concentration was measured for 2 min with the i-STAT.

2.2.3. One-trial passive avoidance test

One-trial passive avoidance tests were conducted as previously described [15]. The apparatus consisted of a two-compartment "light–dark" box (L-D box). The light compartment [9 × 9.5 × 14 (h) cm] consisted of white Plexiglas with a ceiling made of clear Plexiglas, while the dark compartment [14 × 10.5 × 14 (h) cm] was constructed of black Plexiglas and contained a ceiling of the same color. A 5 × 5-cm sliding door connected the two compartments. The floor of the two compartments was constructed of stainless steel rods (5 mm diameter, spaced 10 mm apart). A foot shock (0.3 mA, 3 s duration) could be delivered through the rods of the dark compartment using a shock generator-scrambler (Muromachi-Kikai, Japan, SGS-002).

During the initial habituation trial, mice were placed individually into the light compartment of the L-D box and the sliding door was opened. The mice were allowed to explore in the L-D box for 5 min during which the latency of entering the dark compartment was measured. Mice whose latency exceeded 60 s were excluded from the experiment in order to minimize the deviation of baseline data. Both genotypes of mice were divided into non-stressed and stressed groups (see Table 1) based on their habituation L-D latency to equalize the baseline data. On the day following the habituation trial, an acquisition trial was conducted. The acquisition trial was performed in a manner similar to that of the habituation trial, but the mice received a foot shock immediately upon entrance to the dark compartment. Again, the latency to enter the dark compartment was measured, and mice that did not enter the dark compartment within 60 s were also excluded from the experi-

Table 1
Summary of experiments

Groups	Treatment	Experiment/number of subjects				
		Blood glucose	Passive avoidance	Spontaneous activity	Elevated plus maze	Shock sensitivity
Non-stressed wild	–	5	8	10	9	10
Stressed wild	restraint stress 30 min	6	8	10	10	10
Non-stressed KO	–	6	8	10	9	10
Stressed KO	restraint stress 30 min	6	8	10	10	10

Wild: wild-type mice; KO: NMB-R-deficient mice.

ment. A test trial was conducted 24 h later, and the light–dark (step-through) latency was measured once again. Each trial was terminated at 300 s, and mice that did not enter the dark compartment by this time were assigned a ceiling score of 300 s. After each trial, the apparatus was cleaned using 70% alcohol.

2.2.4. Spontaneous activity test

Spontaneous activity was measured as previously described [21]. Horizontal locomotor activity and vertical movements (rearing and leaning on the wall) of both stressed and non-stressed mice was measured for 30 min using an activity monitoring system [Neuroscience, Japan, test chamber Model ENV-510, 275 × ~275 × ~210 (h) mm; controller Model ENV-50]. After each measurement, the test chamber was wiped with damp towels and 70% ethanol to remove residual odors from urine, feces and sebum. Data were recorded and analyzed with a personal computer. During the experiment, the only light in the room was that from the computer monitor, which mice could not see directly.

2.2.5. Elevated plus maze test

The elevated plus maze test was performed as previously described [23]. The maze (Muromachi-Kikai) was constructed of brown smoke Plexiglas and consisted of a central platform of 9 × 9 cm with four arms radiating from that platform in the shape of a plus. Two opposite arms were open (30 × 6 cm; length × width) while the other two opposite arms (30 × 6 cm) were enclosed by walls of 15 cm (including the end of the arm) with an open top. The maze floor was covered with black rubber, and a raised edge (5 mm) was placed around the perimeter of the open arms to provide additional grip for the animals. The entire apparatus was situated at a height of 40 cm above the floor.

To initiate the elevated plus maze test, an animal was placed on the central platform of the maze facing an open arm. A 5-min test duration was employed and the maze was thoroughly cleaned between tests with damp towels and 70% alcohol to remove residual odors from urine, feces, and sebum. A manually controlled video camera was positioned above the maze at a height of ~1 m at an angle of approximately 50° in relation to the platform and closed arms. Behavior was measured while reviewing the videotape. Behavioral indices used in this study were modified from Dalvi and Rodgers [3] and consisted of the frequency and ratio (%) of open and closed arm entries (arm entry defined as all four paws into an arm), and the duration of staying in open and closed arms. Videotapes were analyzed at least three times by two highly trained observers blinded to the animals' experimental group. Median scores of these VTR analyses were used for statistical analyses.

2.2.6. Measurement of pain response

The shock-sensitivity test was performed as previously described [2]. Pain reactivity was measured using a modification of the flinch-jump test. The floor (20 × 20 cm) consisted of parallel stainless steel rods (5 mm diameter with gaps of 10 mm). Individual animals were placed on the floor, and the apparatus was covered with a 1-l glass beaker, after which six series of six shocks (1-s duration, 20, 40, 60, 80, 100, and 130 μA) were delivered at a 15-s interval through the grid floor. Shock series were administered in double alternating ascending and descending order, the first series being ascending. Shock threshold was defined as the lowest shock intensity (μA) at which an animal's hind foot left the floor. For each mouse a mean shock threshold value was calculated as an average of the six thresholds recorded in the series.

2.3. Statistical analyses

Statistical analyses of blood glucose measurement, spontaneous activity test, elevated plus maze test, and shock sensitivity test were performed using two-way ANOVA, and post hoc analysis were conducted using two-tailed Student's *t* test. Analysis of the one-trial passive avoidance test was performed using two-way ANOVA with repeated measures, and post hoc analyses were conducted using Turkey's multiple comparison method. In the one-trial passive avoidance test, the step-through latency of the acquisition trial and the test trial were compared using the two-tailed Student's paired *t* test.

3. Results

3.1. Blood glucose measurement

Blood glucose concentration is an index of stress response in animals [17], and therefore, glucose concentration was measured in blood samples from NMB-R-deficient and wild-type mice with or without restraint-induced stress (Fig. 1). Two-way ANOVA revealed a significant effect of the genotype [$F(1,28)=11.8$, $P<.002$] and of the stress treatment [$F(1,28)=175.2$, $P<.0001$]. However, the genotype × stress treatment interaction was not significant [$F(1,28)=0.25$]. Post hoc analyses revealed that blood glucose concentration of non-stressed NMB-R-deficient mice was significantly lower than that of wild-type mice ($t=3.23$, $P<.01$). Restraint-induced stress elevated blood glucose concentration in both NMB-R-deficient and wild-type mice (wild-type mice: $t=8.05$, $P<.001$; NMB-R-deficient mice: $t=12.2$, $P<.001$). Furthermore, glucose concentration was also significantly lower in stressed NMB-R-deficient mice compared to the stressed wild-type cohort ($t=2.20$, $P<.05$).

3.2. One-trial passive avoidance test

Results of the one-trial passive avoidance test are summarized in Fig. 2. Two-way ANOVA revealed a significant

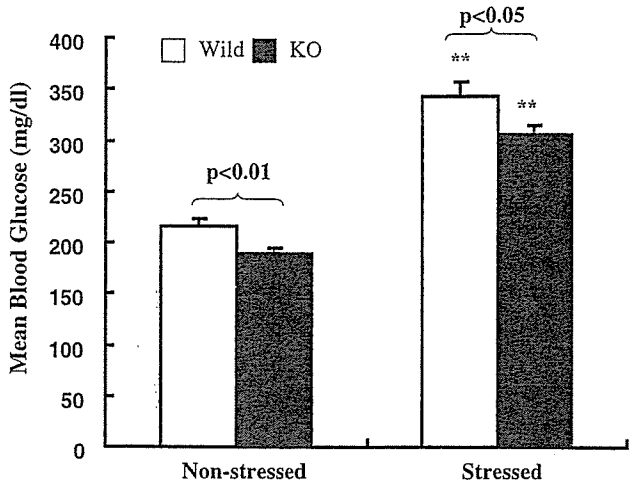

Fig. 1. Measurement of blood glucose levels. Data represent mean+S.E.M. Asterisks indicate statistical difference between the non-stressed and stressed conditions (**: $P<.001$). The P-value indicates statistical difference between wild-type and NMB-R-deficient mice. Wild: wild-type mice; KO: NMB-R-deficient mice.

effect of the trial [$F(1,56)=81.5$, $P<.000001$], of the groups [$F(3,56)=8.61$, $P<.00001$], and a significant trial × group interaction [$F(3,56)=7.78$, $P<.0002$]. No significant differences were observed in the conditioning trial [$F(3,31)=1.02$, n.s.]. In contrast, there was a statistically significant effect of the groups [$F(3,31)=8.25$, $P<.0005$] in the test trial. Post hoc analyses showed no difference ($t=1.10$, n.s.) in the mean step-through latency of non-stressed NMB-R-deficient and wild-type mice, but that for the stressed NMB-R-deficient mice was significantly shorter than the stressed wild-type mice ($t=5.82$, $P<.01$) and non-stressed NMB-R-deficient mice ($t=6.14$, $P<.01$). The step-through latency of test trial was significantly longer than that of the acquisition trial in non-stressed NMB-R-deficient, non-stressed wild-type, and stressed wild-type mice ($t=6.58$, $P<.0005$; $t=4.37$, $P<.005$; $t=5.29$, $P<.002$, respectively), whereas stressed NMB-R-deficient mice did not show a statistical difference between the two trials ($t=2.26$, n.s.).

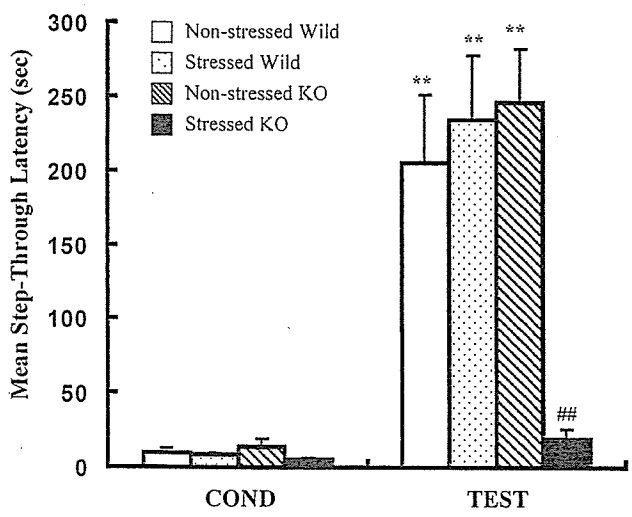

Fig. 2. One-trial passive avoidance test. Data represent mean+S.E.M. Symbols indicate statistical difference between the acquisition trial and the test trial (**: $P<.01$), and between stressed NMB-R-deficient mice and stressed wild-type mice or non-stressed NMB-R-deficient mice in the test trial (##: $P<.01$). COND: acquisition trial; TEST: test trial. Wild: wild-type mice; KO: NMB-R-deficient mice.

3.3. Spontaneous activity test

Fig. 3 shows the results of horizontal locomotor activity. Two-way ANOVA revealed the main effect of genotype [$F(1,36)=0.138$] and of stress treatment [$F(1,36)=2.11$], and the genotype × stress treatment interaction [$F(1,36)=0.25$] were not statistically significant. Post hoc analyses showed no statistical differences between non-stressed NMB-R-deficient and wild-type mice ($t=1.22$) and between stressed NMB-R-deficient and wild-type mice ($t=0.70$). However, stressed NMB-R-deficient and wild-type mice exhibited significantly higher activity than that of the non-stressed cohort ($t=2.78$, $P<.05$; $t=2.38$, $P<.05$, respectively). Vertical movements (rearing and leaning on the wall) were also analyzed and almost identical results were obtained (data not shown).

3.4. Elevated plus maze test

Results of the elevated plus maze test are summarized in Table 2. Two-way ANOVA revealed no statistically significant main effects of genotype and stress treatment and the genotype × stress treatment interaction with respect to the following indices: the number of open arm entries [respectively, $F(1,34)=0.97$; $F(1,34)=1.38$; $F(1,34)=0.588$], the number of closed arm entries [respectively, $F(1,34)=2.23$; $F(1,34)=4.09$; $F(1,34)=0.86$], the percentage of open

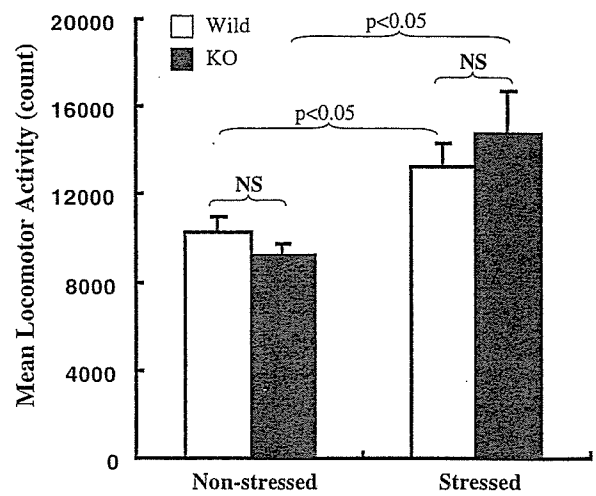

Fig. 3. Spontaneous activity test. Data represent mean+S.E.M. The P-value indicates the statistical difference between non-stressed and stressed NMB-R-deficient mice. NS: not statistically significant. Wild: wild-type mice; KO: NMB-R-deficient mice.

Table 2
Summary of the elevated plus maze test in NMB-R-deficient and wild-type mice with restraint stress

Behavioral index	Non-stressed WT	Stressed WT	Non-stressed KO	Stressed KO
Open arm entries	4.33±1.24	4.70±0.80	2.78±0.57	4.50±0.83
Closed arm entries	7.44±1.32	8.80±1.55	4.44±0.90	8.10±1.03
Total entries	11.8±1.59	13.5±1.80	7.22±1.10	12.6±1.51
% Open entry	34.3±9.52	36.9±5.56	37.1±7.10	34.2±5.46
Time spent in open arms (s)	57.4±23.4	66.1±13.6	45.2±18.4	59.1±12.5
Time spent in closed arms (s)	167.7±24.5	169.0±13.6	164.1±28.3	159.3±17.1
% Time spent in open arms	25.5±10.1	28.0±5.52	23.6±8.44	27.6±5.94

Non-stressed WT: wild-type mice without stress, Stressed WT: wild-type mice with 30-min restraint stress, Non-stressed KO: NMB-R-deficient mice without stress, Stressed KO: NMB-R-deficient mice with 30-min restraint stress. Data represent mean±S.E.M.

arm entries [respectively, $F(1,34)=0.047$; $F(1,34)=0.035$; $F(1,34)=0.36$], the time spent in open arms [respectively, $F(1,34)=0.21$; $F(1,34)=0.56$; $F(1,34)=0.003$], the time spent in closed arms [respectively, $F(1,34)=0.10$; $F(1,34)=0.007$; $F(1,34)=0.022$], and the percentage of time spent in open arms [respectively, $F(1,34)=0.001$; $F(1,34)=0.097$; $F(1,34)=0.049$]. Regarding the total arm entry index, which also represents a form of emotional response of mice to the environment, the main effect of stress treatment was statistically significant [$F(1,34)=5.30, P<.05$]; however, the main effect of genotype and the genotype × stress treatment interaction were not statistically significant [$F(1,34)=3.20$; $F(1,34)=1.41$, respectively]. Post hoc analysis revealed that the number of total arm entry was greater in non-stressed wild-type mice than non-stressed NMB-R-deficient mice [$t=2.36$, $P<.05$] and in stressed NMB-R-deficient than non-stressed mutant mice [$t=2.82$, $P<.05$].

3.5. Measurement of pain response

Fig. 4 shows the results of the shock sensitivity test. Two-way ANOVA did not show a statistically significant main effect of genotype [$F(1,34)=1.41$] and of stress treatment [$F(1,34)=0.26$], and the genotype × stress treatment interaction [$F(1,34)=1.94$].

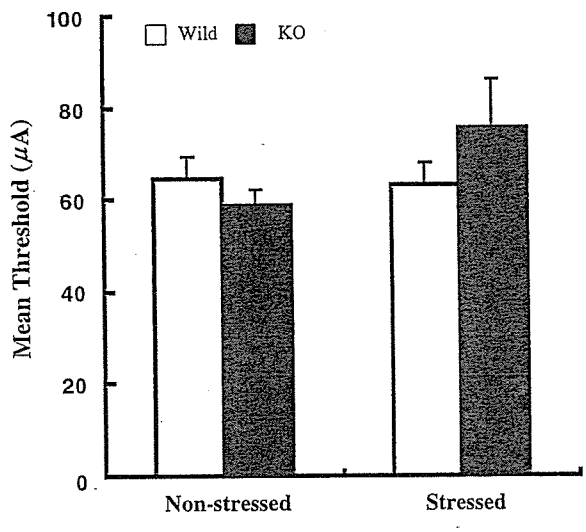

Fig. 4. Shock sensitivity measurement. Data represent mean+S.E.M. Wild: wild-type mice; KO: NMB-R-deficient mice.

4. Discussion

In the present study, we used a relatively mild restraint-induced stress (mice could turn slightly in the direction of their body inside the restraint cage) to examine the effects of stress on behavior in female NMB-R-deficient mice. Administration of a 30-min restraint in a wire mesh cage elicited elevated blood glucose in both NMB-R-deficient and wild-type mice, indicating that this treatment was stressful to the mice (Fig. 1). In the one-trial passive avoidance test, administration of restraint-induced stress prior to conditioning severely impaired memory performance in NMB-R-deficient mice, but not in other groups (Fig. 2). This behavioral change indicates that behavioral responsiveness to stress stimuli may be altered in NMB-R-deficient mice. However, although restraint-induced stress prompted an increase in horizontal locomotor activity and vertical movements in both NMB-R-deficient and wild-type mice, there was no significant difference in activity between stressed NMB-R-deficient and wild-type mice (Fig. 3). Furthermore, an administration of restraint-induced stress did not affect anxiety-related behaviors in an elevated plus maze test (Table 2) and pain response in a shock sensitivity test (Fig. 4) in any group.

The spontaneous activity level of mice is one of the crucial factors that determine performance during learning/memory tasks. Hyperactivity may lead to or coincide with learning deficit [11]. Therefore, we first assessed the effect of stress on spontaneous activity. Restraint-induced stress slightly affected spontaneous activity in both NMB-R-deficient and wild-type mice. However, the elevation of spontaneous activity in stressed NMB-R-deficient mice was relatively moderate and may not have been sufficient to severely impair learning/memory. Further, the activity level of stressed NMB-R-deficient and wild-type mice was not statistically significant. Thus, the elevated activity level after stress could not explain the memory impairment observed in stressed NMB-R-deficient mice.

Anxiety may also contribute to performance during inhibitory avoidance learning. In order to confirm that a

shortening of the step-through latency was not caused by decreased anxiety in stressed NMB-R-deficient mice, we next assessed anxiety in stressed NMB-R-deficient and wild-type mice using the elevated plus maze test paradigm. We recently reported [23] that male NMB-R-deficient mice showed somewhat altered anxiety-related behavior (risk assessment behavior), but exhibited almost normal behavior in the conventional parameters that were used in the present study. Similar to the results with male mice, female NMB-R-deficient and wild-type mice performed nearly the same under stressed and non-stressed conditions. The fact that stressed NMB-R-deficient mice exhibit normal anxiety properties strongly suggests that the observed memory impairment is not a consequence of decreased anxiety.

Pain sensation is another factor that may affect the performance of passive avoidance learning. Many studies report that stress stimuli cause decreased pain sensation in animals (stress-induced analgesia; for a review see Ref. [18]). Here, we assessed the properties of pain sensation in the presence and absence of restraint-induced stress. No differences were observed among groups, and therefore, we excluded the possibility that decreased pain sensation by stress in NMB-R-deficient mice leads to the memory impairment.

As discussed above, memory impairment in stressed NMB-R-deficient mice is not attributable either to increased activity level, decreased anxiety, or decreased pain sensation induced by restraint-induced stress. The near-normal behaviors, which can affect learning and memory indirectly, observed in stressed NMB-R-deficient mice suggest that stress stimuli may affect the regions of the brain and/or the neurotransmission that are closely tied to learning and memory in these mice. Recent studies revealed functional neuroanatomical correlates of the effects of stress and memory (changes in the temporal lobe and hippocampus) [1,7]. Furthermore, NMB-R mRNA is expressed in hippocampal formation and amygdalohippocampal area [20]. Therefore, it may prove fruitful to undertake a detailed analysis of these regions in the stressed NMB-R-deficient mice.

Stress-induced mental disorders, such as the post-traumatic stress disorder, have become a serious social issue. Our present study indicates that NMB-R-deficient mice may constitute a useful animal model for the study of stress-induced mental disorders such as dissociative amnesia seen in survivors of traumatic stress.

Acknowledgements

We thank Dr. M. Yoshida for providing and training regarding the use of i-STAT system. This work was supported in part by research grants from the Ministry of Education, Culture, Sports, Science and Technology and the Ministry of Health, Labour and Welfare.

References

[1] Bremner JD, Krystal JH, Southwick SM, Charney DS. Functional neuroanatomical correlates of the effects of stress on memory. J Trauma Stress 1995;8:527–53.
[2] Cabib S, Castellano C, Patacchioli FR, Cigliana G, Angelucci L, Puglisi-Allegra S. Opposite strain-dependent effects of post-training corticosterone in a passive avoidance task in mice: role of dopamine. Brain Res 1996;729:110–8.
[3] Dalvi A, Rodgers RJ. GABAergic influences on plus maze behavior in mice. Psychopharmacology 1996;128:380–97.
[4] Gross C, Santarelli L, Brunner D, Zhuang X, Hen R. Altered fear circuits in 5-HT_{1A} receptor KO mice. Biol Psychiatry 2000;48: 1157–63.
[5] Itoh S, Takashima A, Itoh T, Morimoto T. Open-field behavior of rats following intracerebroventricular administration of neuromedin B, neuromedin C, and related amphibian peptides. Jpn J Physiol 1994; 44:271–81.
[6] Itoh S, Takahashi A, Itoh T, Morimoto T. Effects of neuromedins and related peptides on the body temperature of rats. Jpn J Physiol 1995; 45:37–45.
[7] Joseph R. The neurology of traumatic "dissociative" amnesia: commentary and literature review. Child Abuse Negl 1999;23:715–27.
[8] Kent P, Anisman H, Merali Z. Are bombesin-like peptides involved in the mediation of stress response? Life Sci 1998;62:103–14.
[9] Lefebvre H, Contesse V, Delarue C, Vaudry H, Kuhn JM. Serotonergic regulation of adrenocortical function. Horm Metab Res 1998;30: 398–403.
[10] Malendwicz LK, Nussdorfer GG. Investigation on the acute effects of neuropeptides on the pituitary-adrenocortical function in normal and cold-stressed rats. I. Bombesin and neuromedin B. Exp Toxicol Pathol 1995;47:31–4.
[11] McDonald MP, Wong R, Goldstein G, Weintraub B, Chen S-Y, Crawley JN. Hyperactivity and learning deficits in transgenic mice bearing a human mutant thyroid hormone β1 receptor gene. Learn Mem 1998;5:289–301.
[12] Merali Z, McIntosh H, Anisman H. Role of bombesin-related peptides in the control of food intake. Neuropeptides 1999;33:376–86.
[13] Minamino N, Kangawa K, Matsuo H. Neuromedin B: a novel bombesin-like peptide identified in porcine spinal cord. Biochem Biophys Res Commun 1983;114:541–8.
[14] Ohki-Hamazaki H, Sakai Y, Kamata K, Ogura H, Okuyama S, Watase K, et al. Functional properties of two bombesin-like peptide receptors revealed by the analysis of mice lacking neuromedin B receptor. J Neurosci 1999;19:948–54.
[15] Santo-Yamada Y, Yamada K, Wada K. Post-training administration of gastrin-releasing peptide (GRP) improves memory loss in scopolamine- and hypoxia-induced amnesic mice. Physiol Behav 2001;74: 139–43.
[16] Saudou F, Amara DA, Dierich A, LeMeur M, Ramboz S, Segu L, et al. Enhanced aggressive behavior in mice lacking 5-HT_{1B} receptor. Science 1994;265:1875–8.
[17] Tabata H, Kitamura T, Nagamatsu N. Comparison of effects of restraint, cage transportation, anaesthesia and repeated bleeding on plasma glucose levels between mice and rats. Lab Anim 1998;32: 143–8.
[18] Takahashi M. Stress-induced analgesia. Yakubutsu Seishin Kodo 1991;11:279–95.
[19] Wada E, Way JM, Shapria H, Kusano K, Lebacq-Verheyden AM, Coy D, et al. cDNA cloning, characterization, and region-specific expression of a neuromedin-B-preferring bombesin receptor. Neuron 1991;6: 421–30.
[20] Battey J, Wada E. Two distinct receptor subtypes for mammalian bombesin-like peptides. TINS 1991;12:524–8.
[21] Yamada K, Ohki-Hamazaki H, Wada K. Differential effects of social isolation upon body weight, food consumption, and responsiveness to

novel and social environment in bombesin receptor subtype-3 (BRS-3) deficient mice. Physiol Behav 2000;68:555–61.
[22] Yamada K, Wada E, Wada K. Bombesin-like peptides: studies on food intake and social behaviour with receptor knock-out mice. Ann Med 2000;32:519–29.
[23] Yamada K, Santo-Yamada Y, Wada E, Wada K. Role of bombesin (BN)-like peptides/receptors in emotional behavior by comparison of three strains of BN-like peptide receptor knockout mice. Mol Psychiatry 2002;7:113–7.
[24] Yamada K, Wada E, Santo-Yamada Y, Wada K. Bombesin and its family of peptides: prospects for the treatment of obesity. Eur J Pharmacol 2002;440:281–90.
[25] Yamada K, Wada E, Yamano M, Sun Y-J, Ohara-Imaizumi M, Nagamatsu S, et al. Decreased marble burying behavior in female mice lacking Neuromedin-B receptor (NMB-R) implies the involvement of NMB/NMB-R in 5-HT neuron function. Brain Res 2002;942:71–8.
[26] Yamada K, Santo-Yamada Y, Wada K. restraint stress impaired maternal behavior in female mice lacking the neuromedin B receptor (NMB-R) gene. Neurosci Lett 2002;330:163–6.
[27] Yamano M, Ogura H, Okuyama S, Ohki-Hamazaki H. Modulation of 5-HT system in mice with a targeted disruption of neuromedin B receptor. J Neurosci Res 2002;68:59–64.

J. Biochem. 132, 245–251 (2002)

Two-Dimensional Electrophoresis/Phage Panning (2D-PP): A Novel Technology for Direct Antibody Selection on 2-D Blots[1]

Masaru Furuta,*,† Takashi Ito,*,† Chikashi Eguchi,*,† Torahiko Tanaka,*,† Eriko Wakabayashi-Takai,*,† and Kiyotoshi Kaneko*,†,[2]

*Department of Cortical Function Disorders, National Institute of Neuroscience, National Center of Neurology and Psychiatry, 4-1-1 Ogawahigashi, Kodaira, Tokyo 187-8502; and †CREST, Japan Science and Technology Corporation, 4-1-8 Honcho, Kawaguchi, Saitama 332-0012

Received March 25, 2002; accepted May 23, 2002

We describe a novel method, two-dimensional electrophoresis/phage panning (2D-PP), for the generation of antibodies against proteins in crude biochemical samples, such as cellular membrane fractions. These sources have traditionally presented problems as to the development of antibodies by conventional techniques. 2D-PP involves two-dimensional resolution of proteins, blotting of the proteins onto a nitrocellulose membrane, and screening of a phage antibody library and isolation of corresponding antibodies. By 2D-PP with detergent-insoluble "lipid rafts" as a target protein complex, we obtained specific phage pools against eight antigen spots (from a total of 39 spots). These antibodies were functional in Western blotting, enzyme-linked immunosorbent assaying (ELISA), and immunoscreening of a cDNA expression library. Propagation of anti-nitrocellulose phages was the major problem in 2D-PP, but was overcome by the use of the soluble anti-nitrocellulose antibody fragment. 2D-PP constitutes a key tool for functional analysis of proteins in complex fractions.

Key words: nitrocellulose membrane, phage display, proteomic analysis, single-chain antibody, two-dimensional electrophoresis.

Currently, major advancements are being made in the field of proteomics with mass spectrometric identification of proteins separated by two-dimensional polyacrylamide gel electrophoresis (2-D PAGE) (*1*). Determination of the physiological roles of such proteins may necessarily require development of specific antibodies against the proteins to allow functional analysis. Advances in the development of antibodies by means of phage display technology are important in such studies since this can be used to produce many functional antibody fragments such as Fab (*2*) or single-chain Fv (scFv) (*3*), the classical hybridoma technology or animal immunization being bypassed (reviewed in Refs. *4* and *5*). Also, antibodies can be selected from phage antibody libraries against molecules that have previously been considered as difficult targets for a conventional immunization method; these molecules include self-antigens (*6, 7*) or cell surface proteins (*8–10*). Here, we describe a novel technology using a phage antibody system to generate antibodies against proteins in a crude biochemical fraction resolved by 2-D PAGE. We have designated the method 2-D electrophoresis/phage panning (2D-PP).

One of the potential problems of phage display technology is a strong bias for developing antibodies against immunodominant antigens when the phage library is screened against highly complexed targets (*11, 12*). To diminish this anticipated bias, we tried to select the binders against each individual component. Proteins in complex biological samples were first separated from each other by 2-D PAGE immobilized on a nitrocellulose membrane, and then each protein was excised and screened by a phage antibody library.

As a target of 2D-PP, we have focused on detergent-insoluble cell membrane microdomains, or lipid rafts, which have been described in prion diseases and Alzheimer's disease (*13*). There is currently no effective method for the isolation of antibodies against proteins separated by 2-D PAGE. Previously, two model studies were reported, in which pure proteins were subjected to 2-D PAGE, eluted from the gel and then used for phage panning (*14, 15*). In our study, we demonstrate the isolation of phage antibodies against unknown 2-D protein spots resolved from a complex lipid raft fraction, and the functional activity of these antibodies in immunobiochemical methods including immunoscreening of a cDNA expression library to identify the target antigens.

MATERIALS AND METHODS

Preparation of 2-D Protein Spots for Phage Panning—Lipid rafts were isolated from human neuroblastoma cell line SK-N-MC (ATCC No. HTB10) as described previously (*16*). Proteins in the fraction were solubilized with 9 M urea, 2 M thiourea, 4% CHAPS, 20 mM Tris-HCl, and 0.5% IPG buffer (Amersham Pharmacia Biotech, Uppsala, Sweden) with vigorous shaking for 1 h, and then subjected to

[1] This work was supported by grants from the Ministry of Health, Labour and Welfare, and the Ministry of Education, Culture, Sports, Science and Technology.

[2] To whom correspondence should be addressed. Phone: +81-42-346-1718, Fax: +81-42-346-1748, E-mail: kaneko@ncnp.go.jp

Abbreviations: ATCC, American type culture collection; Fv, variable region fragment; PBS, phosphate-buffered saline.

isoelectric focusing (the first dimension) with a linear immobilized pH gradient (range, 4–7) and an Immobiline dry strip (Amersham Pharmacia Biotech) according to the manufacturer's protocol. The proteins were then separated by SDS-PAGE (10%) in the second dimension (*17*), and electrotransferred to a nitrocellulose membrane (Hybond-ECL, Amersham Pharmacia Biotech). The 2-D blot was stained with colloidal gold total protein stain (Bio-Rad, Hercules, CA), and each of the visualized protein spots was excised with a Proteome works spot cutter apparatus (Bio-Rad) the diameter being 1 mm.

Phage Panning with 2-D Protein Spots—Phage antibodies were selected through 5 rounds of panning from the human synthetic single-chain Fv (scFv) library (Griffin.1 library, provided by Dr. G. Winter, MRC, Cambridge, UK, http://www.mrc-cpe.cam.ac.uk/~phage/), where basic manipulations of phages were performed according to the protocols for the library ("the library protocol," http://www.mrc-cpe.cam.ac.uk/~phage/g1p.html). For the experiments on each target antigen, four pieces of the excised protein spots were incubated with 1×10^{12} cfu of phage pool in each round. The experimental conditions for panning were as follows: method [i] is an original protocol and several modifications have been made to method [ii] to suppress the propagation of anti-nitrocellulose phages. A soluble anti-nitrocellulose scFv fragment was prepared from the anti-nitrocellulose phage obtained in this study according to the library protocol.

Method [i]: Protein spots were blocked with 10% skim milk in PBS (MPBS) containing 25% glycerol, and then incubated with phages (1×10^{12} cfu) in 1 ml of 10% MPBS containing 0.1% Tween 20 (MPBST) for 1 h. Then the spots were washed three times with PBS containing 0.1% Tween 20 (PBST) for 5 min, five times with 10% MPBS containing 25% glycerol for 20 min, and finally three times with PBS for 5 min. The bound phages were eluted with 100 mM triethylamine and propagated according to the library protocol.

Method [ii]: The antigen spots were first soaked in PBS containing 1% Tween 20 for 1 h for renaturation of the blotted proteins (*18*), and then blocked with 10% MPBST supplemented with a soluble anti-nitrocellulose scFv fraction. Next, phage antibodies (1×10^{12} cfu) in 200 μl of 10% MPBST supplemented with anti-nitrocellulose scFv were reacted with the antigen spots overnight (round 1) or for 3 h (rounds 2–5). Protein spots were washed once with PBS (round 1), or washed three times with PBST for 5 min and once with PBS for 5 min (rounds 2–5). In rounds 4 and/or 5, the anti-nitrocellulose scFv was omitted from the blocking and phage reactions. Bound phages were eluted as above.

Purification of ScFv—The scFv used in this study is tagged with a histidine hexamer and secreted into culture supernatant when expressed in *Escherichia coli* (see the library protocol). The secreted scFv was purified with a metal affinity resin (TALON™; Clontech, Palo Alto, CA) according to the manufacturer's protocol.

DNA Finger Printing of Phage Clones—The scFv insert of each phage clone was amplified by PCR (*19*) using primers 5′-CGGATAACAATTTCACACAGGAAAC (sense) and 5′-CTATGCGGCCCCATTCAGATC (antisense). The products were digested with *Hae*III and the restriction patterns were analyzed by agarose gel electrophoresis.

Phage Western Blotting—The lipid raft fraction was subject to SDS-PAGE (1-D) or 2-D PAGE, and then electroblotted onto nitrocellulose membranes. The membranes were stained with colloidal gold (Bio-Rad), renatured as described above (when needed), and then blocked with 10% MPBST for 1 h. Then the membranes were incubated with phages (5×10^{10} cfu/ml) in 10% MPBST for 1 h and washed with PBST three times for 5 min each. The membranes were incubated with anti-M13 antibodies conjugated with peroxidase (Amersham Pharmacia Biotech) in 1:7,000 diluted 5% MPBST for 1 h and washed as above. The bound phages were visualized with ECL Western blotting detection reagents (Amersham Pharmacia Biotech).

Immunoscreening of a cDNA Expression Library with Phage Antibodies—A human brain 5′-stretch plus λTriplEx cDNA library (Clontech) was screened with the phage antibodies isolated in this study. The λ phage plaques were grown and transferred to a Hybond-ECL nitrocellulose membrane according to the manufacturer's protocol. The screening with phage antibodies was carried out in the same manner by phage Western blotting, as described above.

Phage ELISA—A 96-well plate (Corning, Corning, NY) was coated with each of the following antigens (50 μg/ml, dissolved in PBS): human vimentin (Progen, Heidelberg, Germany), bovine actin (Sigma), human thyroglobulin (Biogenesis, England, UK), bovine serum albumin (BSA, Life Technologies), and hen egg-white lysozyme (ICN Biomedicals, Aurora, OH). After blocking with 10% MPBS for 1 h, monoclonal phage antibodies mo17–2 and mo23–7 (1×10^{10} cfu in 100 μl 10% MPBS) were incubated in each well for 1 h. After washing, 1:7,000 diluted anti-M13 peroxidase-conjugated antibodies (Amersham Pharmacia Biotech) were reacted in the wells for 1 h. After washing of the wells, bound phages were detected with an ABTS substrate kit (Nacalai Tesque, Kyoto).

Mass Spectrometry—The 2-D protein spots visualized with a copper staining kit (Bio-Rad) were cut out and subjected to in-gel digestion with trypsin (*20*). The masses of tryptic peptides were determined with a MALDI-TOF (matrix-assisted laser desorption/ionization-time of flight) (*21*) mass spectrometer (Voyager RP, Applied Biosystems), and peptide mass fingerprinting analysis was performed with MS-FIT software.

RESULTS

The lipid raft fraction is enriched with cholesterol, sphingolipids, and associated proteins such as glycosylphosphatidylinositol (GPI)-anchored, doubly acylated or transmembrane proteins, and is characterized by insolubility in nonionic detergents such as Triton X-100 (*22–24*). This feature makes the protein components in lipid rafts hard to analyze in an aqueous solution. However, lipid rafts could be analyzed successfully using 2D-PP, in which the target antigens were immobilized on a nitrocellulose membrane during the antibody screening.

We used human synthetic scFv library Griffin.1 for phage antibody screening. For optimization of the conditions of 2D-PP, phage antibodies against BSA and thyroglobulin were isolated from the library by panning with polystyrene tubes (Maxisorp™; Nalgenunc, Rochester, NY) according to the library protocol. To find the membrane most suitable for the phage reaction, four different membranes

(nitrocellulose, PVDF, negatively-charged PVDF and nylon) were subjected to dot blot analysis using anti-BSA phages (Fig. 1A). Among them, nitrocellulose membranes gave the best contrast between the positive and negative signals of chemiluminescence, the others showing higher levels of background phage binding. Next, the blocking effect of the skim milk concentration on Western blotting was examined. The phage antibody specific to a non-raft protein, thyroglobulin, was reacted with a 1-D blot of lipid raft proteins in the presence of 0–10% skim milk. As shown in Fig. 1B, the nonspecific binding of anti-thyroglobulin phage to raft proteins was completely blocked in the presence of 10% skim milk. Furthermore, we determined the concentrations of phages suitable for panning with the membrane. Various concentrations of anti-BSA and irrelevant (anti-thyroglobulin) phages were reacted with BSA blots in 10% skim milk, and then the titers (colony forming units, cfu) of the bound phages were compared between the specific and irrelevant phages (Fig. 1C). The amounts of specific phages bound to BSA were higher than those of irrelevant phages at any concentrations of phages. The ratio between the specific and nonspecific phage binding (specific/nonspecific) became larger with higher concentrations of the phages: 13 at 10^{10} cfu/ml and 37 at 10^{12} cfu/ml. Thus, we employed higher concentrations of phages (10^{12} to 10^{13} cfu/ml) for the reaction with antigen spots. We also checked the effect of a high concentration (25%) of glycerol (25) in the blocking and washing steps of panning on the selection of positive phages. As a model experiment, the excised 2-D blot of BSA on nitrocellulose was screened for the Griffin.1 library. As shown in Table I, clones specific to BSA were more effectively enriched in the presence of glycerol in the blocking and washing steps than in its absence of glycerol: 24 out of 24 clones were specific after the 5th round of panning with glycerol.

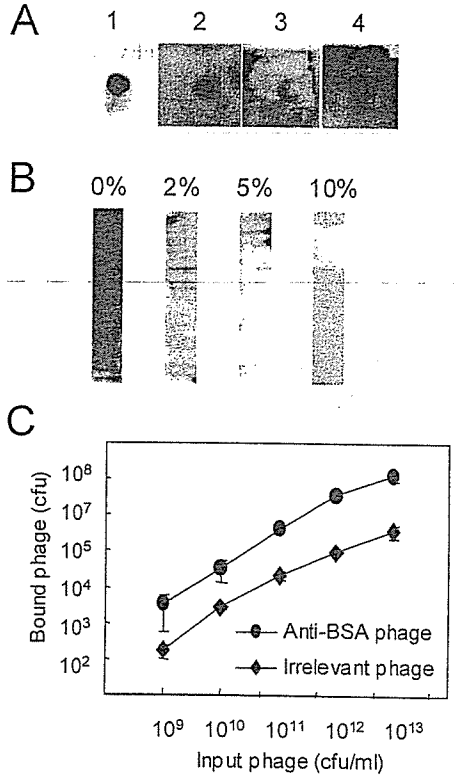

Fig. 1. **Optimization of conditions for phage panning.** (A) Difference in phage detection on chemically distinct membranes. BSA (50 ng) was dotted onto the following membranes, (1) nitrocellulose (Hybond-ECL), (2) PVDF (Fluorotrans, Pall, East Hills, NY), (3) negatively charged PVDF (Fluorotrans G, Pall), and (4) nylon (Biodyne A, Pall), and then blocked with 5% skim milk and incubated with anti-BSA phage (10^{11} cfu/ml) for 1 h. After washing, phage binding was evaluated by chemiluminescent detection as described under "MATERIALS AND METHODS." (B) Blocking effect of skim milk on Western blotting with phage antibodies. After blocking with various concentrations of skim milk, a 1-D blot of the lipid raft fraction on a nitrocellulose membrane was reacted with phages specific to a non-raft protein, thyroglobulin. (C) Evaluation of the optimal phage concentration for phage binding to an antigen blot. An excised nitrocellulose membrane (1 mm in diameter) was coated with BSA (100 μg/ml), and then reacted with various concentrations of phages after blocking with 10% skim milk. Bound phages were eluted with 100 mM triethylamine and titrated according to the library protocol. Values are the means ± SD of 3 independent experiments.

TABLE I. **Effect of glycerol in the blocking and washing steps on 2D-PP.**

Conditions for blocking and washing	Frequency of positive phage clones				
	Rounds of selection				
	1	2	3	4	5
With glycerol[a]	–	–	1/24	1/24	24/24
Without glycerol[b]	–	–	1/24	3/24	5/24

Phages (1×10^{12} cfu/ml in 10% MPBST) were panned against an excised 2-D blot of BSA using the Griffin.1 library. After each round, 24 phage clones were analyzed by *Hae*III fingerprinting and the specificity to BSA was checked for the unique clones by dot blot analysis. [a]Blocked for 1 h with 10% MPBST containing 25% glycerol. Washed 3 times for 5 min with PBST, 5 times with 10% MPBST containing 25% glycerol, and 3 times for 5 min with PBS. [b]Blocked for 1 h with 10% MPBST. Washed 3 times for 5 min with PBST.

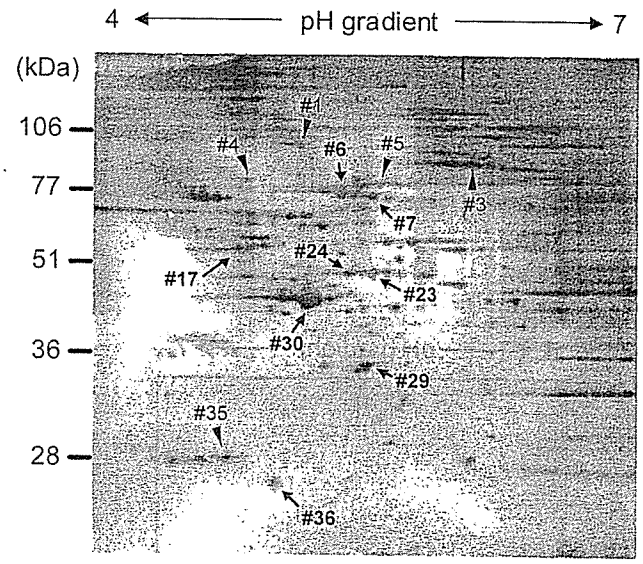

Fig. 2. **2-D PAGE of lipid rafts (160 μg as protein).** The protein spots on a nitrocellulose membrane were visualized by colloidal gold staining. The antigen spots against which phage antibodies were generated in this work are indicated by arrows. The spots indicated by arrowheads are the proteins identified by mass spectrometry.

Based on these results (Fig. 1 and Table I), we decided experimental conditions such as the incubation conditions and the number of panning rounds for method [i] described in "MATERIALS AND METHODS."

As the antigen source for panning, the lipid raft fraction of human neuroblastoma SK-N-MC cells was subjected to 2-D PAGE and then transferred to a nitrocellulose membrane. The protein spots were visualized by colloidal gold staining, since it exhibits high sensitivity comparable to that of silver staining of polyacrylamide gel (nanogram amounts of proteins are detectable) and is not known to have an inhibitory effect on antibody binding (*26–28*). We detected about 200 individual protein spots on the 2-D membrane (pH 4–7) with 160 μg protein of lipid rafts (Fig. 2). Since the nitrocellulose itself had the potential for antigenicity in our preliminary experiments, each antigen spot was excised (1 mm in diameter) and used for the phage reaction. The 32 antigen spots (#1–#32) that were detectable in every run were initially subjected to phage panning using the Griffin.1 library with original protocol method [i] (see "MATERIALS AND METHODS"). The enrichment of the specific binders in phage pools was evaluated by 1-D Western blotting of the lipid raft fraction (Fig. 3A). After 5 rounds of selection, specific antibodies were generated to three antigen spots, #17, #23, and #24 (3/32, 9.4%). We failed to obtain specific binders to other antigens, while the propagation of anti-nitrocellulose phages was observed in 25 antigen spots (25/32, 78.1%), such as #6, #7, #19, and #30 (Fig. 3A). No binders were enriched on the remaining four antigens (for example, spot #20).

We tried modification of the panning procedure in order to reduce the anti-nitrocellulose binders and to recover specific binders more efficiently (method [ii], see "MATERIALS AND METHODS"). To achieve optimum binding of specific phages to the antigens, renaturation treatment of antigen spots with Tween 20 (*18*) was introduced to each round of panning. To compete with anti-nitrocellulose phages, a soluble anti-nitrocellulose scFv fraction was added for the blocking and phage reactions.

Using the total 36 protein spots (#1–#39 except for #17, #23, and #24), the 5 rounds of panning with Tween 20 treatment and anti-nitrocellulose scFv were again per-

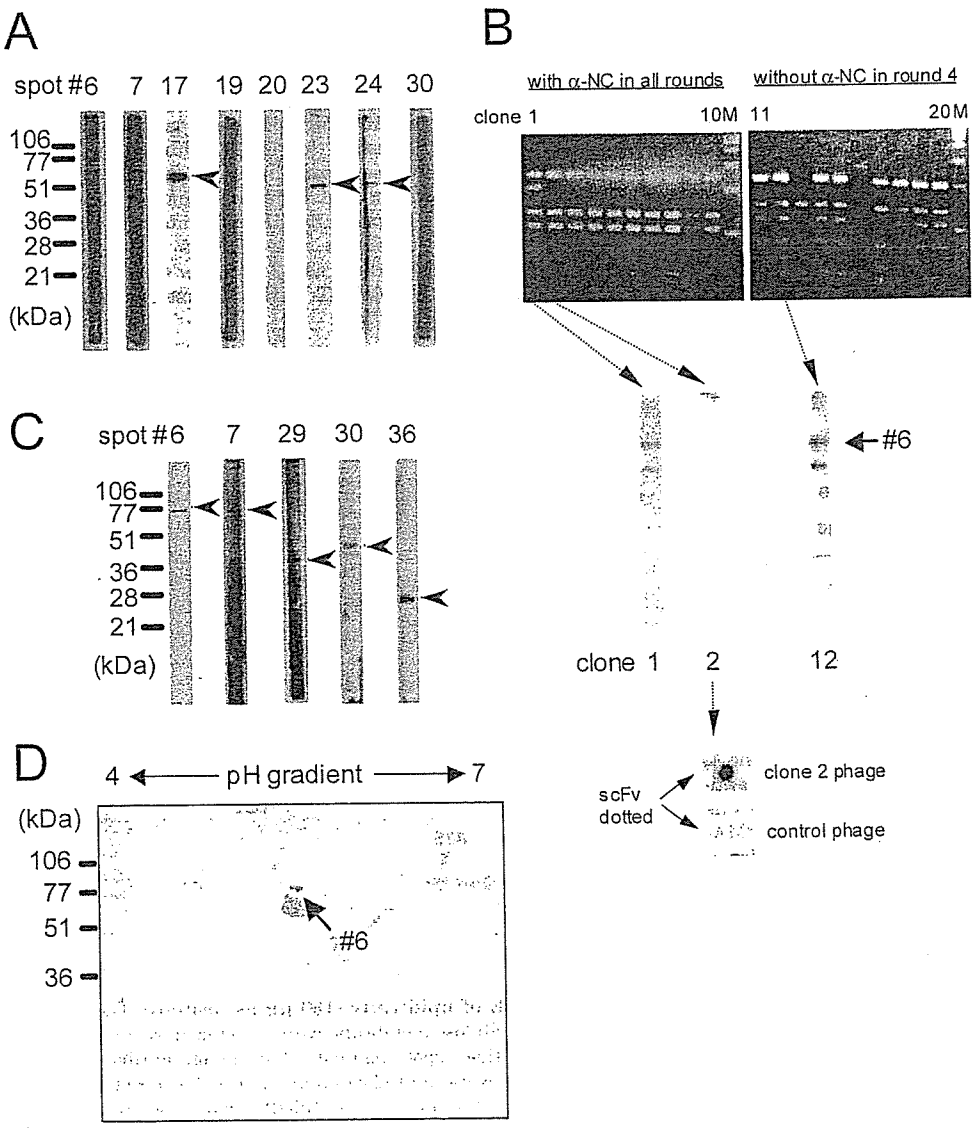

Fig. 3. **Characterization of phage antibodies isolated by 2D-PP against lipid raft proteins.** (A) 1-D Western blotting using polyclonal phage pools selected by means of method [i]. The signals corresponding to the target antigens are indicated by arrowheads. (B) Effects of the anti-nitrocellulose scFv fraction (α-NC) on phage panning. Top; the phage library was panned by means of method [ii] for 5 rounds against spot #6 with α-NC in all rounds (left) or with α-NC in all rounds except round 4 (right). *Hae*III fingerprinting of 10 randomly chosen phage clones is illustrated for each experiment (clones 1–10 and 11–20). M, DNA size markers. Middle; 1-D Western blotting with representative monoclonal phages. Bottom; dot blot analysis of purified scFv (anti-thyroglobulin) with clone 2 and control phage antibodies. (C) 1-D Western blotting using polyclonal phages selected by means of method [ii]. The protein bands corresponding to the target antigens are indicated by arrowheads. (D) 2-D Western blotting using the polyclonal phage pool against spot #6.

formed. When the soluble anti-nitrocellulose scFv was added through all 5 rounds, anti-nitrocellulose backgrounds were not detected on Western analysis. However, phages against the scFv dominated over the specific phage antibody clone, which were presumably selected and expanded against the anti-nitrocellulose scFv fraction. A representative experiment is illustrated in Fig. 3B: the dominant clones on spot #6 (clones 2–10 on fingerprinting, the top panel) are not reactive with the antigen on 1-D Western blotting (middle panel) but with scFv (dot blot presented at the bottom), indicating that the dominant clone was an anti-scFv phage. Only clone 1 reacted with the #6 antigen (middle panel).

We then performed the panning in the absence of anti-nitrocellulose scFv in round 4 or 5 (or both). This procedure sufficiently suppressed the predomination of anti-scFv phages and the most dominantly enriched clone on spot #6 (clone 12) showed binding to the #6 antigen (Fig. 3B). We employed these experimental conditions for the final panning procedure, method [ii]. We applied method [ii] to the panning on 36 antigen spots (#1–#39 except for #17, #23, and #24), and reactive phage antibodies were newly obtained against 5 antigen spots, #6, #7, #29, #30, and #36 (5/36, 13.9%) (Fig. 3C). Anti-nitrocellulose phages, however, were enriched on 28/36 spots (77.8%), suggesting that the anti-nitrocellulose phages potentially propagated even in the presence of anti-nitrocellulose scFv. The rest (3/36) showed no signal. Each of the polyclonal phage pools obtained by 2D-PP was functional in 2-D Western blotting, as expected. A representative blot experiment is illustrated in Fig. 3D. The specific phage pool reacted with multiple spots of the same molecular weight (#6), suggesting that the #6 antigen was modified, such as by phosphorylation.

The phage antibodies obtained in this work were applied to the immunoscreening of a cDNA expression library to identify its target antigens. Since the phages were selected against antigens immobilized on nitrocellulose membranes and fully functional on Western blotting, these antibodies were expected to recognize polypeptides immobilized on nitrocellulose on immunoscreening. Using monoclonal phage antibodies mo7–4.16 and mo17–2 (specific to spot #7 and #17, respectively), 1×10^6 λ clones of the human brain cDNA expression library were screened. For each phage antibody, one or two immunopositive λ phage plaques were isolated and their insert sequences were determined. On the BLAST (basic local alignment search tool) (29) search of nucleotide sequence databases, antigen #7 was identified as annexin VI and #17 as vimentin. In order to verify these results, we performed 2-D Western blotting and ELISA using their commercial antibodies and antigens. The antibodies against annexin VI or vimentin specifically reacted with spot #7 (Fig. 4A) or #17 (not shown) respectively, on the 2-D blot of lipid rafts. Phage antibody mo17–2 specifically reacted with human vimentin on ELISA (Fig. 4B). We

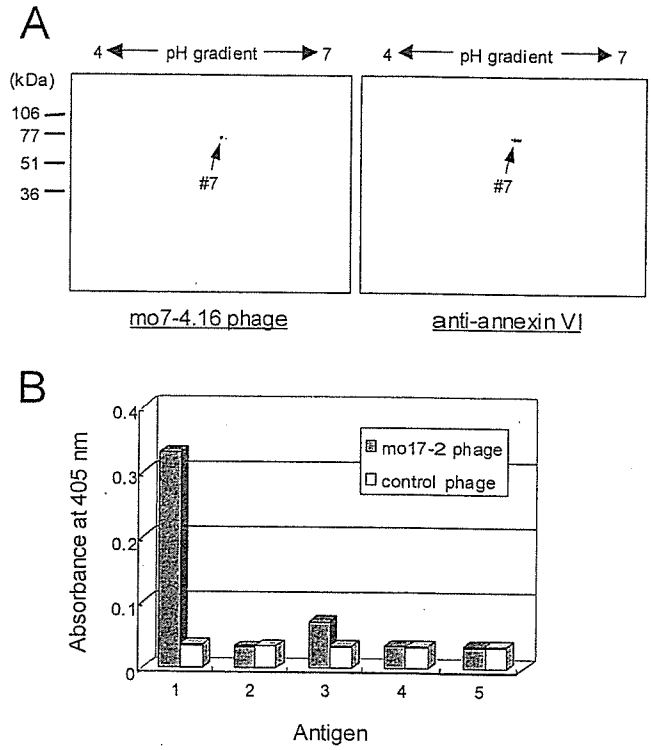

Fig. 4. **2-D Western blotting and ELISA using anti-#7 and #17 phage antibodies.** (A) 2-D Western blotting using anti-#7 monoclonal phage mo7–4.16 (left) and commercial anti-annexin VI (right) antibodies. (B) Specific binding of monoclonal phage antibody mo17-2 to vimentin on ELISA. The binding of phage clones mo17–2 and mo23-7 (control) was determined, by ELISA, to vimentin (1) and unrelated proteins (2–5); actin (2), thyroglobulin (3), bovine serum albumin (4), and hen egg-white lysozyme (5).

TABLE II. **Profiles of lipid raft proteins on 2D-PP.**

Antigen spot	Selection method[c]	Identification[d]	Molecular weight (kDa)	Isoelectric point	Average hydrophobicity[f]
#17[a]	[i]	Vimentin	53.7	5.06	−0.823176
#23[a]	[i]	Ubiquinol-cytochrome *c* reductase core I protein	52.6	5.94	−0.135417
#24[a]	[i]	Ubiquinol-cytochrome *c* reductase core I protein	52.6	5.94	−0.135417
#6[a]	[ii]	Vacuolar ATPase (isoform VA68)	68.3	5.35	−0.189951
#7[a]	[ii]	Annexin VI	75.9	5.42	−0.451560
#29[a]	[ii]	G protein β2 subunit	37.3	5.60	−0.177059
#30[a]	[ii]	Actin	41.7	5.29	−0.199733
#36[a]	[ii]	n.i.	27[e]	5.0[e]	–
#1[b]	–	Neuronal kinesin heavy chain	117.4	5.65	−0.744575
#3[b]	–	α-1 Catenin	100.1	5.95	−0.367550
#4[b]	–	Tumor rejection antigen (gp96) 1	92.5	4.76	−0.712703
#5[b]	–	DnaK-type molecular chaperone	73.7	5.87	−0.523197
#35[b]	–	SNAP-23	23.4	4.89	−0.810426

[a]To which the specific phages were generated in this study. [b]Randomly chosen. [c]See "MATERIALS AND METHODS." [d]Antigens #7 and #17 were identified by immunoscreening and the others by mass spectrometry. [e]Apparent values on the 2-D gel. [f]Calculated with the SOSUI system. n.i., not identified.